Scientific Papers of
the Department of Electrical Power Engineering of
the Wrocław University of Technology

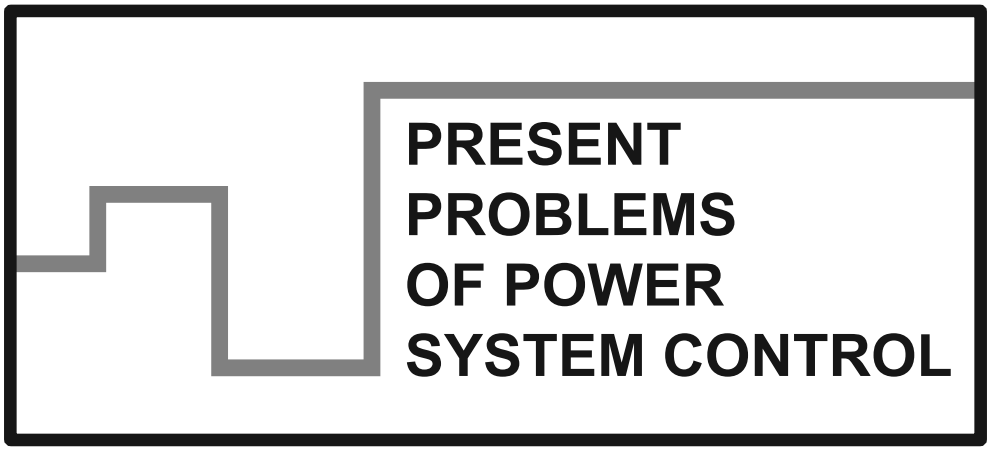

6

Wrocław 2015

Printed in the camera ready form

Department of Electrical Power Engineering
Wrocław University of Technology
Wybrzeże Wyspiańskiego 27, 50-370 Wrocław, Poland
phone: +48 71 320 35 41
www: http://www.weny.pwr.edu.pl/instytuty,52.dhtml; http://www.psc.pwr.edu.pl
e-mail: wydz.elektryczny@pwr.edu.pl

OFICYNA WYDAWNICZA POLITECHNIKI WROCŁAWSKIEJ
Wybrzeże Wyspiańskiego 27, 50-370 Wrocław
http://www.oficyna.pwr.edu.pl
e-mail: oficwyd@pwr.edu.pl
zamawianie.ksiazek@pwr.edu.pl

ISSN 2084-2201

Print and binding: beta-druk, www.betadruk.pl

CONTENTS

K. SOLAK, W. REBIZANT, Study of Ferroresonance Phenomena in HV Power Networks 5
T. LAZIMOV, E. SAAFAN, Influence on Heterogeneous Earth Layers Parameters' Contrast on Ground Return Impedance 15
R. CZECHOWSKI, E. ROSOŁOWSKI, ITC System Security in the Context of Contemporary Challenges for Electric Power Industry 21
P. REGULSKI, Estimation of Composite Load Model Parameters as a Constrained Nonlinear Problem 33
J. IŻYKOWSKI, E. ROSOŁOWSKI, P. PIERZ, Analysis of Ferroresonance Oscillations in Capacitive Voltage Transformer 43

inductive voltage transformer,
ferroresonance oscillations;
high voltage networks; simulation,

Krzysztof SOLAK*
Waldemar REBIZANT*

STUDY OF FERRORESONANCE PHENOMENA IN HV POWER NETWORKS

Analysis of ferroresonance phenomena in high voltage (HV) power networks is presented in this paper. The adequate digital simulation model for investigation of ferroresonance oscillations in MATLAB/Simulink program was developed. In the paper HV power system configuration with circuit breaker grading capacitors was described and analyzed. The phase as well as open delta VT voltages and their spectra were considered as signals for ferroresonance detection. Additionally, the possibility of ferroresonance oscillations suppression was also studied.

1. INTRODUCTION

The ferroresonance oscillations may occur in configurations where a nonlinear inductance (e.g. representing magnetizing branch of a voltage transformer, VT or CVT, power transformer, etc.) is connected to the power system capacitance (e.g. capacitance of cable or transmission line, reactive power compensation capacitor bank, circuit breaker grading capacitors, etc.), [1, 2]. The series (voltage) ferroresonance arises when capacitance is series connected to the nonlinear inductance, while the parallel (current) ferroresonance takes place for parallel configuration of capacitance and the nonlinear inductance. These nonlinear phenomena can occur in ungrounded or grounded neutral systems, both in medium voltage and high voltage power networks. Typical power system configurations, where ferroresonance oscillations are highly likely, are presented in details in [1, 3]. Generally, ferroresonance oscillations can be initiated by even small change of system parameters or during transients, e.g. one- or two-pole switching operations, fuse blowing, transient phase-

* Wrocław University of Technology, Department of Electrical Power Engineering, Wybrzeże Wyspiańskiego 27, 50-370 Wrocław, Poland, e-mail: krzysztof.solak@pwr.edu.pl

to-ground fault, lightning, transformer switching, loss of system grounding [1, 2]. The ferroresonance phenomenon is complex due to its nonlinearity that brings several steady-state responses, high level of signals (voltage and current) and content of many different frequencies.

Commonly, four types of ferroresonance oscillations may be distinguished, if the spectrum content is taken into account, [1]:

- fundamental mode: the signal waveforms are periodic and their spectra are discontinuous; the signal period is the same as power system period T_1 which means that fundamental frequency component f_1 dominates in signal spectrum that additionally may contain large number of harmonics (e.g. $2f_1$, $3f_1$, ...);
- subharmonic mode: for this condition the signal waveforms are also periodic, whereas the period of signal is a multiple of the system frequency period which brings period equal to nT_1 (n is integer) and frequencies being equal f_1/n; the signal spectrum comprises subharmonics f_1/n (usually odd order, n = 3, 5, 7) and fundamental component f_1;
- quasi-periodic mode: the signal is non-periodic for this state and its spectrum is also discontinuous, the frequency spectrum consists of a number of frequencies (at least two components) which corresponds to a linear combination of formula $nf_A + mf_B$ (where coefficients n and m are integers and the ratio of f_A/f_B is a non-integer value); generally, for this mode the fundamental component and subharmonics may occur;
- chaotic mode: for this state the signal waveform is non-periodic and its spectrum is continuous in broad band – in the other words it looks like high level of noise contained in frequency spectrum.

The ferroresonance phenomenon can be recognized by frequency spectrum analysis of voltage and current signals as well as Poincaré map or phase plane diagram.

It can be concluded that non-linear oscillations can be characterized by overvoltage, overcurrent and waveform distortions (by subharmonic and higher frequencies). This disturbance may be dangerous for power system elements because it increases the thermal (by overcurrent) and electrical (by overvoltage) stresses that may destroy VTs or other equipment as well as distort voltage and current measurement, which may affect the protection operation.

The problem with ferroresonance oscillation in power systems has not been solved yet due to its complex behavior resulting from its non-linear and random nature. Therefore, there is still a need for analysis of ferroresonance phenomena and study of suppression methods of these oscillations.

In this paper results of analysis of ferroresonance oscillations in HV network and typical methods of suppression of this phenomenon are demonstrated. In Section 2, the MATLAB/Simulink digital model of the HV power system to study ferroresonance and analysis of non-linear oscillations results are described. Next (Section 3), selected method of ferroresonance oscillations suppression is presented that is based on intro-

duction of a damping resistance in open delta VT circuit. Lastly, Section 4 presents the conclusions of this work.

2. FERRORESONANCE STUDIES FOR HV POWER SYSTEM MODEL

Typical HV power system configuration, where ferroresonance oscillations are highly likely, comprises circuit breaker grading capacitors and inductive voltage transformers connected in parallel with zero sequence network capacitance [1, 4]. The grading capacitors are mounted in parallel with each arcing chamber of circuit breaker. The main purpose of use of the grading capacitors is to equalize the voltage distribution across the chambers, which increases the switching capacity of the breaker.

For the analysis of ferroresonance phenomenon a simplified model of HV power system shown in Fig. 1 was developed in ATP/EMTP environment [5]. As one can see, this is an HV network with grounded neutral where VTs are in parallel with the zero sequence network capacitance. In addition, circuit breaker is equipped with grading capacitors in order to increase its switching capacity. The VTs were modeled as three single-phase saturable transformers with voltage ratios assumed $400/\sqrt{3}$ / 0.1/3 kV/kV. The primary windings of VTs were connected in grounded Wye while the VTs secondary windings were connected in open delta. The VT model includes appropriate nonlinear magnetizing characteristic. The source impedance Z_S was calculated for the short circuit capacity assumed at the level 250 MVA. The ferroresonance under simulation was initiated by opening circuit breaker grading capacitors at t = 0.2s.

The value of CB grading capacitance C_g was assumed to be 600 pF while the value of phase-to-ground capacitance C_0 was in the range from 50 pF to 5000 pF in increments of 10 pF.

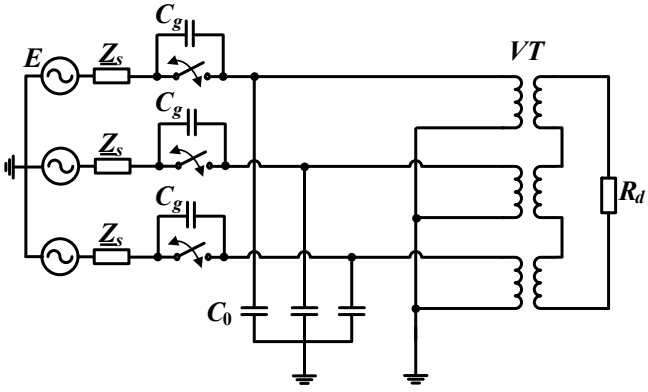

Fig. 1. Basic HV power system for ferroresonance studies – ATP/EMTP model

It is proposed that the ferroresonance oscillations are to be recognized by analysis of spectrum of the voltages in three phases and voltage in open delta VT connection. For this purpose 240-point DFT (Discrete Fourier Transform) was applied. It was assumed that sampling frequency equals 1000 Hz, which means that 240 points (samples) in terms of time correspond to 0.24 s. In such a case the signal spectrum consists of spectral lines regularly spaced at the frequencies distant by 1000/240 = 4.17 Hz. The figures below show the spectra of the voltages in three phases and the voltage in open delta VT connection calculated after opening circuit breaker and for steady-state.

The voltage spectra for cases of opening circuit for assumed range of zero sequence network capacitance C_0 are depicted in Fig. 2. It is clearly seen that ferroresonance oscillations occurred – fundamental frequency component does not only predominate in voltage spectrum after opening circuit breaker but also overvoltage is observed. After analysis of graphs presented in Fig. 2 one can conclude that frequencies of 16.67 Hz, 50 Hz and 150 Hz predominate after ferroresonance oscillations inception (amplitudes of spectral lines are greater than 0.3pu, see especially Fig. 2d). Additionally, in Fig. 3 one can see that what frequencies predominate in the voltage (in open delta VT connection) depends on the value of phase-to-ground capacitance C_0. The frequencies of 50 Hz, 150 Hz and 250 Hz predominate in voltage spectrum for phase-to-ground capacitance between 140 pF to 850 pF (Fig. 3a). Note that according to above definition this is the fundamental ferroresonance because fundamental frequency component and also odd harmonics (especially 3rd) were observed. The frequencies lower than 50 Hz predominate for phase-to-ground capacitance C_0 between 3000 pF to 3400 pF (Fig. 3b) and also in the range from 4160 pF to 4430pF (Fig. 3c). It can be noted that for these values of capacitance C_0 the subharmonic ferroresonance takes place with 3rd subharmonic predominating in voltage spectrum (see Fig. 3c – amplitude of spectral line is the highest for frequency of 16.67 Hz).

Generally, two types of ferroresonance oscillations (fundamental and subharmonic) were observed and the amplitudes of spectral lines (except for the one of 50 Hz) are less than 1.0 pu. It can be noted that for other values of phase-to-ground network capacitance the ferroresonance oscillations are not stable, which means that they have occurred (subharmonic, quasi-periodic and chaotic ferroresonance were observed), however they lasted for very short time and after this the considered HV power system came back to its normal 50Hz steady-state. Such situation is clearly visible in Fig. 4 where chaotic ferroresonance oscillations took place after opening circuit breaker, they lasted for 2.1s and then the system jumped back into its normal 50Hz steady-state. The chaotic mode was recognized since the spectrum of voltage in phase L1 is distributed continuously from 0 to 400 Hz (see Fig. 4).

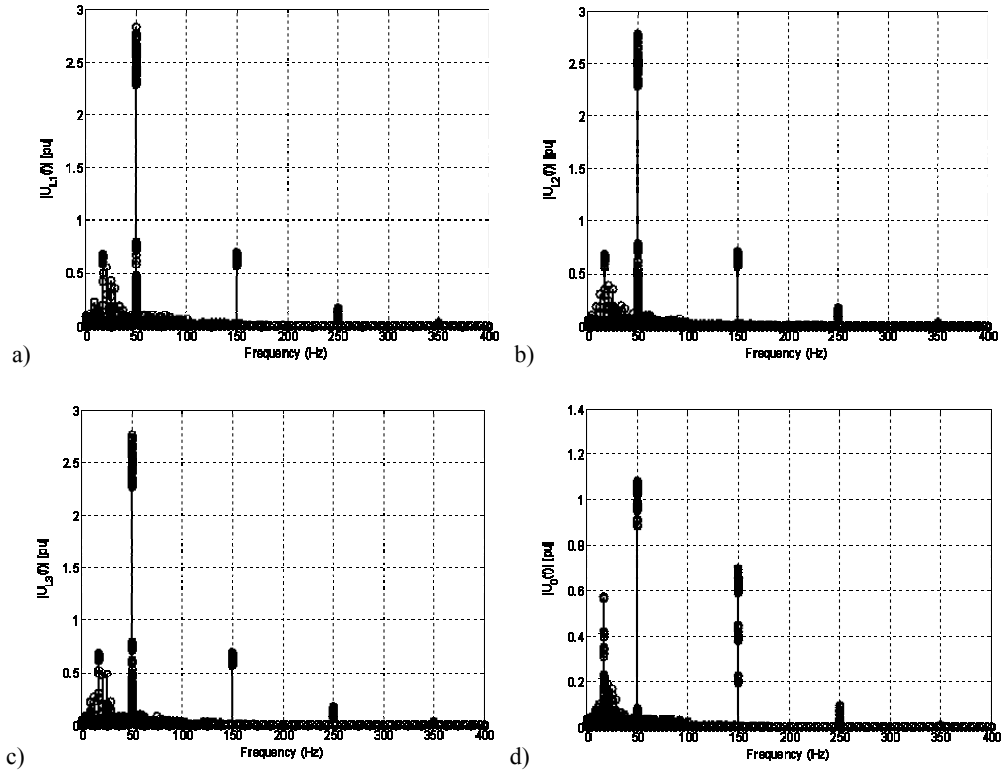

Fig. 2. Spectrum of voltage (after opening circuit breaker): a) in phase L1, b) in phase L2, c) in phase L3, d) in open delta VT connection

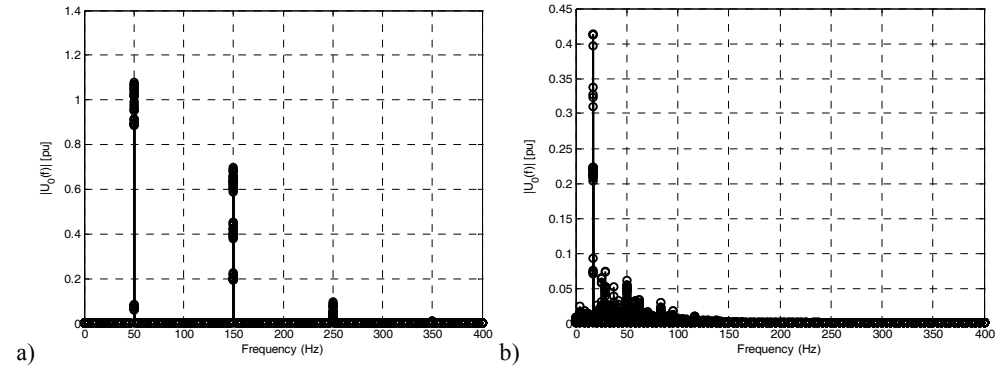

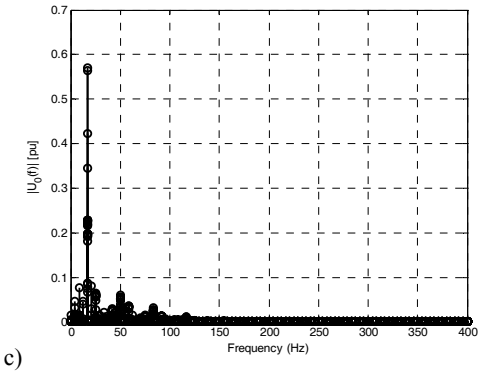

c)

Fig. 3. Spectrum of voltage (after opening circuit breaker) in open delta VT connection for: a) phase-to-ground capacitance C_0 between 140 pF and 850 pF, b) phase-to-ground capacitance C_0 from 3000 pF to 3400 pF, c) phase-to-ground capacitance C_0 between 4160 pF and 4430 pF

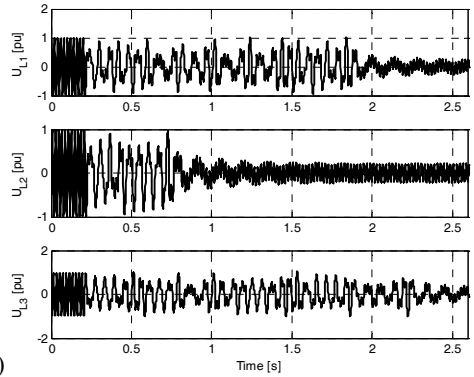

a)

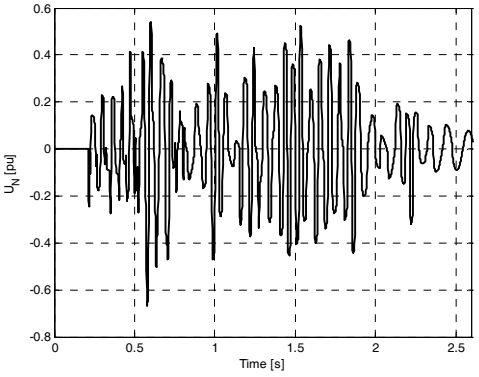

b)

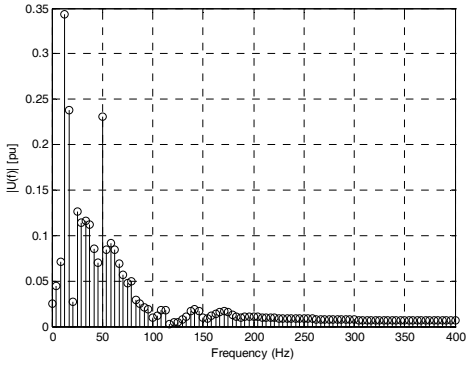

c)

Fig. 4. Case of opening circuit breaker for phase-to-ground capacitance C_0 = 2120 pF: a) three phase voltages, b) voltage in open delta VT connection, c) spectrum of voltage in phase L1

3. SUPPRESSION OF FERRORESONANCE OSCILLATIONS

The possibility of ferroresonance oscillations suppression was also studied and the results are presented in this section. In practice, the ferroresonance oscillations can be suppressed by temporary connection of additional suppressing resistance R_{d1} to the VTs' open triangle (Fig. 5). This method is advantageous since the VTs are thermally stressed only for a short period of time. However, this manner requires an algorithm for detection of ferroresonance oscillations.

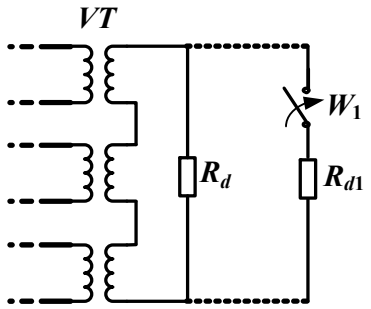

Fig. 5. Method of ferroresonance oscillations suppression

In the literature [6] it is proposed to calculate the value of damping resistance R_{d1} according to the following formula:

$$R_{d1} = \frac{3\sqrt{3}U_S^2}{P_e} \tag{1}$$

where: U_S – secondary voltage of VT (here: 100/3 V), P_e – rated thermal limit burden. The rated thermal limit burden can be calculated by multiplying the total rated burden of VT (here 100 VA) by square of a so called voltage factor. This voltage factor equals to 1.5 for systems with grounded neutral, while for ungrounded systems it should amount to 1.9 [7]. The suppressing resistance (1) is very simple to calculate since all necessary parameters are easily available.

For the considered HV system the damping resistance calculated from (1) was $R_{d1} = 26\ \Omega$. This value of resistance was adopted for testing of the proposed suppression method. In addition, closing times (time during which the damping resistance is connected to VTs' open triangle) $t_{close} = 0.2$, 1.0 and 1.5 s were considered.

The effectiveness of ferroresonance oscillations suppression for cases when ferroresonance was caused by opening circuit breaker is presented in Fig. 6. The presented graphs show that ferroresonance oscillations were not suppressed effectively

for the whole assumed range of C_0 (especially for phase-to-ground capacitance between 140 pF to 850 pF, where fundamental mode dominates). It can be concluded that extension of closing time from 0.2 s to 1.5 s did not help much. Therefore, the only way to improve the suppression effectiveness is lowering of the suppressing resistance.

Figure 7 presents the effectiveness of suppression for the same situation as the former one but with suppressing resistance R_{d1} = 0.25 Ω. It can be observed that ferroresonance oscillations were suppressed effectively for nearly whole range of C_0 (it is still problem with suppression of fundamental mode ferroresonance oscillations). Note that for closing time of t_{close} = 1 s the best results were obtained (Fig. 7b).

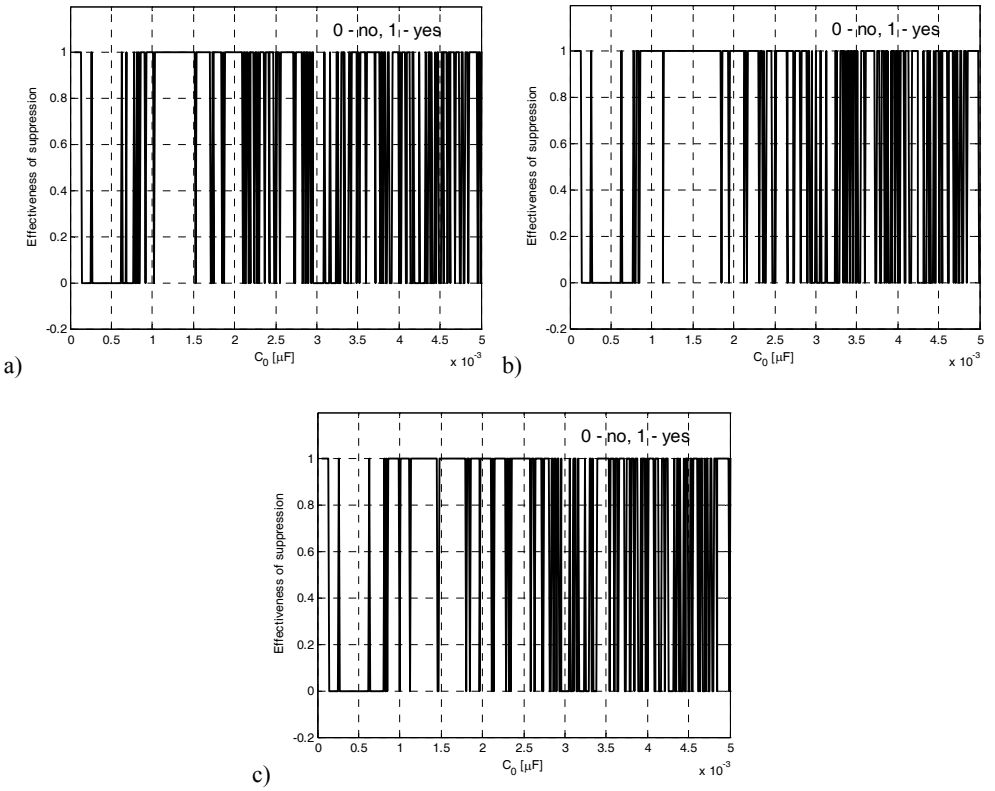

Fig. 6. Ferroresonance oscillations initiated by opening circuit breaker – effectiveness of suppression vs. C_0 for suppressing resistance R_{d1} = 26Ω and: a) t_{close} = 0.2 s, b) t_{close} = 1 s, c) t_{close} = 1.5 s

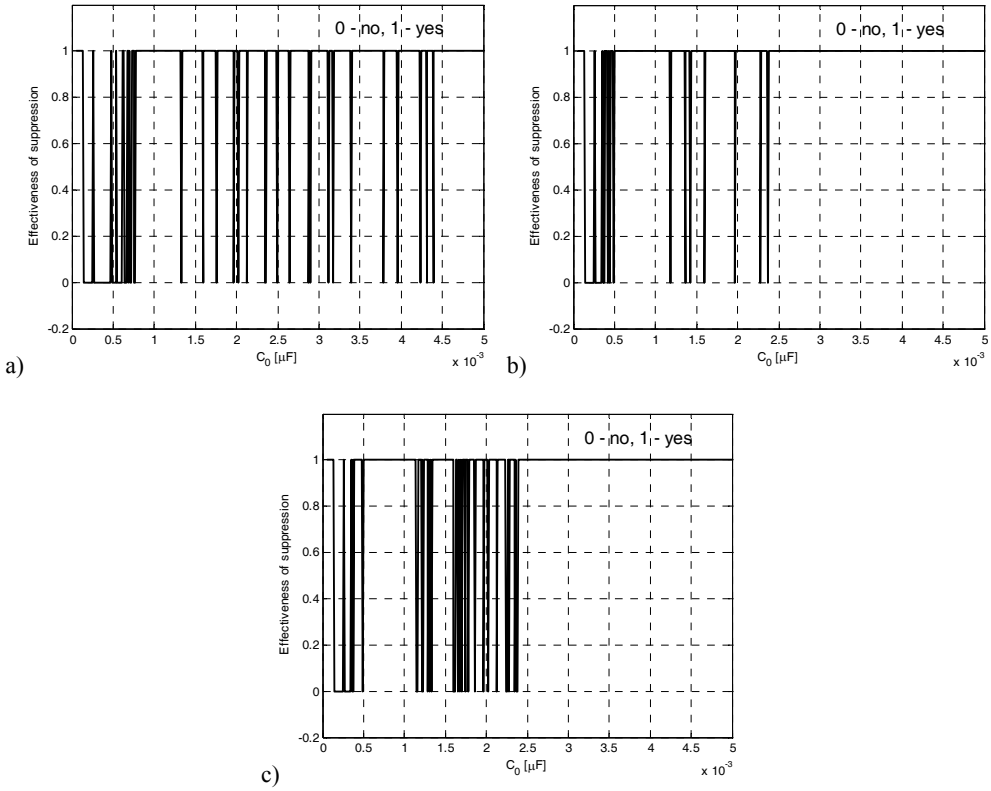

Fig. 7. Ferroresonance oscillations initiated by opening circuit breaker – effectiveness of suppression vs. C_0 for suppressing resistance $R_{dl} = 0.25\ \Omega$ and: a) $t_{close} = 0.2$ s, b) $t_{close} = 1$ s, c) $t_{close} = 1.5$ s

4. CONCLUSIONS

In this paper the problems with ferroresonance phenomenon in HV grounded neutral systems are described. After analysis of the simulation results it could be noticed that initiation of the ferroresonance oscillations in HV grounded neutral power systems is quite possible. However, it is observed mostly in configurations where VTs are in parallel with the zero sequence network capacitance and the circuit breaker is equipped with grading capacitors. It can be noted that for such configuration of HV power system the fundamental and subharmonic ferroresonance oscillations were observed. In addition, chaotic ferroresonance also took place, however it was characterized as a quickly disappearing transient.

Additionally, the ferroresonance oscillations suppression possibility was studied. The testing results prove that it is difficult to suppress ferroresonance oscillations by

temporary switching of suppressing resistance in VTs' open triangle. One can conclude that the most promising results are obtained for very low value of suppressing resistance R_{d1} = 0.25 Ω and closing time of 1.0 s. However, for the assumed suppressing resistance the VTs could be thermally highly stressed, therefore additional studies and/or experiments related to VTs durability for such conditions ought to be performed.

REFERENCES

[1] FERRACCI P., *Ferroresonance, Cahier technique no 190*, Groupe Schneider, March 1998.

[2] IRAVANI M.R. et al., Slow Transients Task Force of the IEEE Working Group on Modelling and Analysis of System Transients Using Digital Programs, *Modelling and Analysis Guidelines for Slow Transients* – Part III: *The Study of Ferroresonance*, IEEE Trans. on Power Delivery, Vol. 15, No. 1, January 2000, pp. 255–265.

[3] HORAK J., *A review of ferroresonance*, 57th Annual Conference for Protective Relay Engineers, 30 March–1 April 2004, pp. 1–29.

[4] Val ESCUDERO M., DUDURYCH I., REDFERN M.A., *Characterization of Ferroresonant Modes in HV Substation with CB Grading Capacitors*, International Conference on Power Systems Transients (IPST '05), Montreal, Canada, 19–23 June 2005, Paper No. 146.

[5] DOMMEL H.W., *Electromagnetic Transients Program. Reference Manual (EMTP theory book)*, Bonneville Power Administration, Portland 1986.

[6] SANAYE-PASAND M., REZAEI-ZARE A., MOHSEN H.,, FARHANGI Sh., *Comparison of Performance of Various Ferroresonance Suppressing Methods in Inductive and Capacitive Voltage Transformers*, Proceedings of the IEEE Power India Conference, New Delhi, 2006.

[7] IEC 60044-2, *Instrument transformers* – Part 2: *Inductive voltage transformers*, 2003.

Carson problem, ground return impedance,
horizontally-layered earth, penetration depth

Tahir LAZIMOV*, Esam SAAFAN*

INFLUENCE OF HETEROGENEOUS EARTH LAYERS PARAMETERS' CONTRAST ON GROUND RETURN IMPEDANCE

Aerial electrical line's impedances of ground return through heterogeneous and homogeneous grounds and their differences were calculated for the earth with different interlayer contrast of parameters for series thicknesses of the earth upper layer. Behavior of the impedance differences against changes of frequency and upper layer's depth is investigated in the article. It was shown that the worst approach of relative differences to the zero takes place for the little thicknesses of the earth upper layer (less than 8 meters) and very high frequencies at which the impedance concept loses its certainty and physical meaning.

1. INTRODUCTION

The problem under consideration had been started to be studied in 1926 when John Carson published his known article [1]. In the minded article J. Carson presented a new formula and got it's presentations for argument's little and high bands. The formula expresses earth contribution into some parameters (such as electrical field intensity, magnetic vector potential, ground return parameters [1-4]) of double-wired electrical line passing above homogeneous ground. The Carson formula does not take into consideration dielectric properties of ground. By this reason it cannot be adequate enough for higher frequencies when longitudinal displacement currents cannot be neglected.

* Electric Supply and Insulation Chair, Azerbaijan Technical University, AZ1009, Baku, Azerbaijan, tahirlazim@gmail.com

**Electrical Engineering Department, Faculty of Engineering, University of El-Mansoura, Box 35516, Egypt, esam_ali_saafan@yahoo.com

The formula obtained by W. H. Wise [5] is adequate for wider frequency bands because of taking into consideration the dielectric properties of ground via dielectric permittivity appeared in the expression (1) given below. The maximum frequencies provided adequacy at use the Wise formula are estimated in [6]. Note that both Carson and Wise formulae concern just to the cases of homogeneous ground.

$$Z = R + j\omega L = j\frac{\omega\mu}{\pi}\int_0^{\infty}\frac{e^{[-(h_m+h_n)\lambda]}\cos(a\lambda)}{\lambda+\sqrt{\lambda^2+j[\omega\mu\gamma+j\omega^2\mu(\varepsilon-\varepsilon_0)]}}d\lambda \tag{1}$$

In the previous formulae Z is so called modified linear impedance, Ohm/m; R is ground return resistance – real component of Z, Ohm/m; j is imaginary unit; ω is electromagnetic field angular frequency, rad/s; determined via linear frequency f as $\omega=2\pi f$, Hz; μ is magnetic permeability, H/m; h_m and h_n are the mean highs of the two-wired system conductors with indexes m and n, m; a is the projection of distance between these conductors to the horizontal plane, m; γ is conductivity of ground, S/m.

A modification of the Wise formula for horizontally-layered ground expressed as following:

$$Z = R + j\omega L = j\frac{\omega\mu}{\pi}\int_0^{\infty}\frac{e^{[-(h_m+h_n)\lambda]}\cos(a\lambda)}{\lambda+\frac{\sqrt{\lambda^2+j[\omega\mu\gamma_1+j\omega^2\mu(\varepsilon_1-\varepsilon_0)]}}{A}}d\lambda \tag{2}$$

The function *(A)* is so called ground impedance expressed in accordance with [7] as,

$$A = \coth\left[-jk_1d+\coth^{-1}\sqrt{\frac{K_1}{K_2}}\right] \tag{3}$$

where K_1 and K_2 are the wave factors of the upper and lower layers equaled respectively,

$$K_1 = \sqrt{-(\gamma_1+j\omega\varepsilon_1)(j\omega\mu_1)} \tag{4}$$

$$K_2 = \sqrt{-(\gamma_2+j\omega\varepsilon_2)(j\omega\mu_2)} \tag{5}$$

here ε is dielectric permittivity, F/m; $\varepsilon_o=10^{-9}/(36\pi)$ F/m is the dielectric constant, d is thickness of the upper layer, m.

Note here that as it was shown in [8] this integral does not exist in the terms of general value. By this reason numerical calculation of the Carson integral for electrically heterogeneous ground becomes more important.

In some cases for calculation the Carson integral for heterogeneous (horizontally-layered) earth may be used its principal value that was obtained in [7].

2. RESULTS OBTAINED

Let us consider the following two structures of heterogeneous earth strongly differed by layers parameters' contrast. The upper layer for both structures is water with $\gamma_u = 0.02$ S/m; $\varepsilon_{u,r} = 80$; d = 5, 8, 10, 20, 50 and 200 m.

a) For the more contrast case select the parameters of the lower layer $\gamma_l = 0.0001$ S/m, $\varepsilon_{l,r} = 9$ corresponded to granite. For this case the maximum difference between impedance of layered and homogeneous grounds changes between 81 – 160 % in the band of frequencies from 50 Hz to 3 - 5 MHz. Frequencies appropriated to the maximum differences lie in the band 50 Hz – 20 kHz.
b) For the less contrast case select the parameters of the lower layer $\gamma_l = 0.01$ S/m, $\varepsilon_{l,r} = 15$ corresponded to clay. For this case the maximum difference between impedance of layered and homogeneous grounds changes between 48 – 88 % in the band of frequencies from 50 Hz to 3 - 5 MHz. Frequencies appropriated to the maximum differences lie in the band 500 Hz – 1 MHz.

Both cases are illustrated in the fig.1 and fig.2 respectively. There has taken place no good behavior of the relative differences function against frequency at little depths of upper layer (less than 8 meters) for both cases (more and less contrast of the multi-layered ground's parameters). As it is seen from the results obtained the relative differences of impedance become negligible at higher depths for the frequencies in the band 20 kHz - 1 MHz. In contrast, big differences have been occurred at less depth that contradicts with the physical nature of the phenomenon under consideration. We think that this has computational character conditioned by change of physical conditions of electromagnetic waves' propagation.

It is known that the concept of impedance is determined and valid for the plane electromagnetic wave. It is also known that at frequencies about 4 – 5 MHz electromagnetic radiation should not be neglected and the concept of impedance loses its meaning. We think this may explain unusual behavior of relative difference at high frequencies (more than 4 – 5 MHz) for the little thickness of the upper layer. According to formula (6) given below table 1 shows the frequencies appropriated to the penetration depths equaled to the upper layer thicknesses. The frequencies shown are higher (for the little thicknesses of the upper layer) than the valid range mentioned

above. As a result, the relative differences of impedance for depths less than 8 meters have a behavior deviated from the expected one.

$$\lambda = \frac{c}{f\sqrt{\varepsilon_{u,r}}}$$

$$d = \lambda$$
$$f = \frac{c}{d\sqrt{\varepsilon_{u,r}}} \tag{5}$$

Table 1. Frequencies corresponded to penetration depths' equaled to the upper layer thickness

λ, m	5	8	10	20	50	200
f, MHz	6.70	4.19	3.35	1.68	0.670	0.168

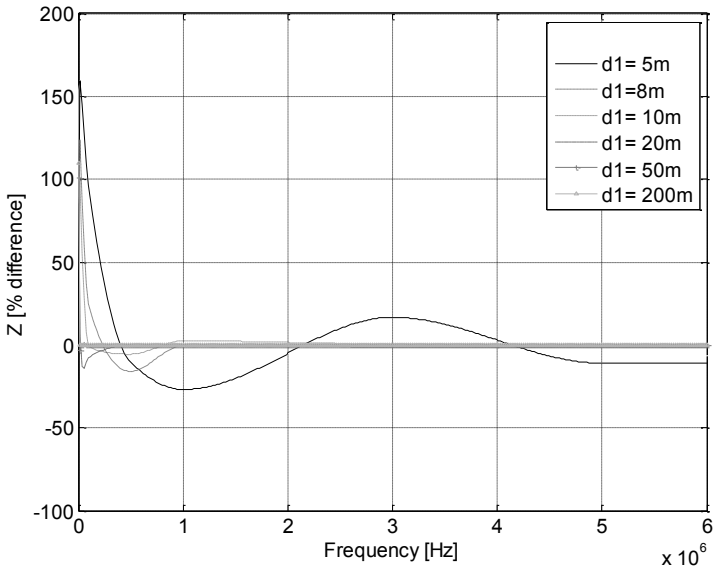

Fig. 1. Relative differences of impedance for the more contrast case

It is known that the electrical nature of substance may be evaluated by comparison of active conductivity γ and capacitive conductivity $(\omega\varepsilon)$. Dependently on relation between these parameters (>>, >, < or <<) a substance may be classified as conductor, bad conductor, bad dielectric and dielectric respectively [9].

For the contrast estimation between layers parameters for both cases use comparison of upper and lower layers conductivities (active and reactive). By using the ratio $\gamma/(\omega\varepsilon)$ to estimate the interlayer contrast for the cases under consideration, the ratio estimated is expressed as $(\gamma_u \varepsilon_l)/(\gamma_l \varepsilon_u)$. Thus for the more and less contrast cases we get the ratios of interlayer contrast equaled to 22.5 and 0.375 respectively. It means that contrast between the cases considered equals 22.5/0.375 = 60.

Note that as it is seen from the fig. 1 and fig. 2 greater thicknesses of the earth upper layer are characterized with better approach of the relative differences curves to zero. We explain this with relative decreasing of the penetration depth in comparison with upper layer thickness.

The results obtained are well-corresponded to other ones got in our previous researches of the problem under consideration given in [10, 11].

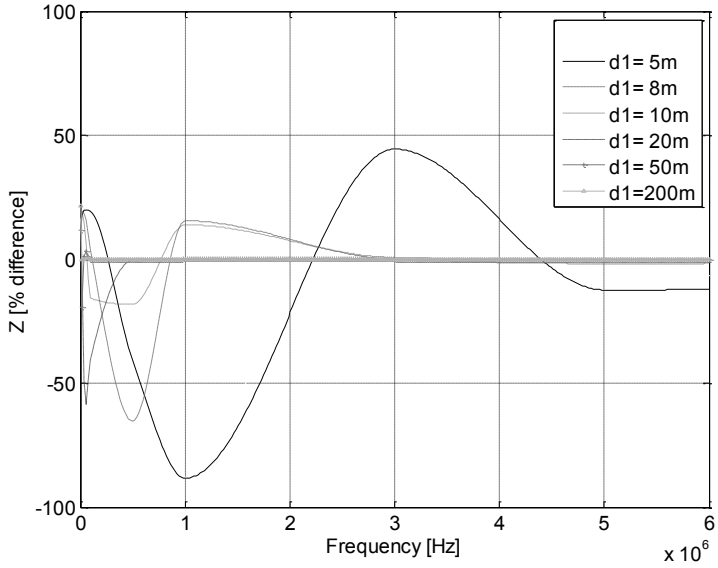

Fig. 2. Relative differences of impedance for the less contrast case

3. CONCLUSIONS

Interlayer contrast of heterogeneous earth parameters influences on difference between ground return impedances calculated for homogeneous and heterogeneous (two-layered for the considered problem) earth. The degree of this influence is rather weak because that increasing the contrast in the dozens of times leads to a change in the minded difference in tens of percent.

REFERENCES

[1] J. R. Carson, *Wave propagation in overhead wires with ground return*, The Bell System Technical Journal, Vol. 5, No. 4, pp. 539-554, 1926.

[2] V. R. Bursian, *Theory of electromagnetic fields used in electrical exploration*, Leningrad: Nedra, 1972 (in Russian).

[3] M. V. Kostenko, *Mutual impedances between overhead lines taking into account skin-effect*, Electricity, No. 10, pp. 29-34, 1955 (in Russian).

[4] T. M. Lazimov, *Analytical expression of Carson integral for electrically homogeneous ground*, Electricity, No. 8, pp. 66-72, 1993 (in Russian).

[5] W. H. Wise, *Propagation of free frequency currents in ground return systems*, Proceeding IRE, Vol. 22, No. 4, pp. 522-527, 1934.

[6] T. M. Lazimov, *Analytical expression for the resistance of electrically homogeneous ground taking account its dielectric properties*, Russian Electrical Engineering (New-York edition), Vol. 66, No. 2, pp. 27-31, 1996.

[7] V. I. Glushko, *Methods for calculation magnetic influence between electric circuits taking into account finite conductance of earth*, Electricity, No. 3, pp. 6-18, 1986 (in Russian).

[8] T. M. Lazimov, *On convergence of Carson integral for horizontally layered earth*, Balkan Journal of Electrical & Computer Engineering, Vol. 1, No. 1, pp. 2-5, 2013.

[9] Jian-Ming Jin, *Theory and computation of electromagnetic fields*, Illinois University: Wiley, 1962.

[10] T. M. Lazimov, E. Saafan, *Some Features of Double-Wired Aerial Line's Ground Return Impedance Calculation at Taking into Consideration Multi-Layered Earth's Structure*, AASCIT Physics, Vol.1, 2, pp.102-106, 2015.

[11] T. M. Lazimov, E. Saafan, *Some Modeling Features of Horizontally-Layered Ground's Return Parameters*, Balkan Journal of Electrical & Computer Engineering, Vol. 3, No. 2, pp. 50-54, 2015.

smart power grid, digital security, transport protocol,
smart metering, remote control, security policy

Robert CZECHOWSKI*
Eugeniusz ROSOŁOWSKI*

ITC SYSTEM SECURITY IN THE CONTEXT OF CONTEMPORARY CHALLENGES FOR ELECTRIC POWER INDUSTRY

In recent years, electric power systems, in order to improve their efficiency, are increasingly using the latest innovations in the field of information and communication technologies (ICT) starting from wireless communication and fiber optics systems. Both used for industrial automation purposes and complex data analysis. Those systems, year by year, have made use of more and more sophisticated communication algorithms leading to automatic management of energy distribution process as well as undertaking the system resuscitation tasks as a result of failure. The use of ICT communication equipment in electric power systems is certainly a big advantage, but it also entails some safety issues. The traditional understanding of smart grid cyber security involves the general requirements (placed on existing systems) as well as specific solutions for detection and intrusion prevention (for individual parts of the system infrastructure). Implementation of security policy in management process of the power system, with means of modern technical of digital information transmission, will increase efficiency and reliability of those systems.

1. INTRODUCTION

Electric power systems are currently the highest priority organisms in the hierarchy of state stability assurance. They are referred to as critical systems for a reason. Their proper functioning, entailing production and distribution of electricity, has to be backed by tested management solutions and, more importantly, by utilization of latest technical solutions, not only in terms of business organization concept but also fitting these networks with advanced control and measurement systems. Not so long ago, communication of individual devices installed in a SCADA (*Supervisory Control and Data Acquisition*) central system operator's substations was done entirely based on

* Wrocław University of Technology, Department of Electrical Power Engineering, Wybrzeże Wyspiańskiego 27, 50-370 Wroclaw, Poland, e-mail: robert.czechowski@pwr.edu.pl

serial communication by use of an often specific and dedicated infrastructure. Interestingly enough, the initial expansion stage of these electronically advanced devices included creation of many mutually incompatible standards along with unusual communication interfaces. Producers used the interchangeably, which did not allow for a single leading standard to spread, and, on top of that, they were wrongly convinced that more advanced devices using closed protocols, the basis for their digital communication, would lead to standardization of their technology. An additional problem was often limitations resulting from the protocols themselves, physical interfaces and limited cable length (supplied by the producer) used to connect and run these devices. A few years ago, it was a very common practice to move data from one system to another – usually by use of external storage media. That phenomenon was noticed by companies specializing in production of unusual interface converters that made it possible to transmit signals via a transmission medium convenient to the operator. A definitely better solution which, despite of its simplicity, performed the function of industrial automation remote administration tool was commonplace opening of backdoors in the form of VPN (*Virtual Private Network*) tunnels. Not so long ago, in the scale of digital technology development, a very popular program in industrial automation was Real VNC (*Virtual Network Computing*) [1]. It was widely and recklessly used by novice electrical power system administrators, which led to diminished security level, not only automation and control systems, but also tele-information ones. It was often forgotten (in a rush of emotions associated with the launch of the service) that utilization of virtual tunnels comes with a certain degree of risk. On one hand, we acquire remote control of a distant automation surveillance system, but on the other, that often unsecured system becomes a proverbial gateway for people we would rather not have access our network. Many people forgot to disable the possibility of communication with programs from outside the local network, change the default communication ports or limit communication of the technological process supervising station to a minimum by way of traffic filtering or limiting the number and types of ports allowing for communication with a specific system interface. The above solution was very troublesome, especially for those local businesses and companies whose control and measurement stations were located all over the city (often distanced by several kilometers from each other), an integration of those systems into a single, cohesive one, controlled from one place, was no small challenge.

2. DEVELOPMENT OF TELE-INFORMATION IN ELECTRICAL POWER SYSTEMS

Utilization and popularization of solutions from commonly understood teleinformatics make the development of electrical power systems, in this regard, head in a completely new direction. Their structure already resembles that of modern tele-

information networks – ICT (*Information and Communication Technologies*). Considerable development of information technologies (IT), especially tele-information networks with different scope and area of functionality (LAN, MAN, WLAN and WWAN networks) will allow for fully automatic and remote control of control and measurement systems. Additionally, development of such areas as complex networks will allow control systems for autonomous decision making based on current events and pre-defined rules. A different issue, also being another direction for development of Smart Power Grids (SPG), is not only data analysis but also data mining [2]. Such a process will provide the electric power system operator with completely new information they would not be able to see in a traditional electric power system model. Skillful utilization of this information will allow for not only accurate knowledge and understanding of one's own network's operational logic, but also some real benefits: decreased energy consumption during peak hours, decreased losses due to automated energy balance and increased security of the energy transfer itself. Utilization of IT technologies will contribute to more efficient management of these networks. Unfortunately, their ill-conceived utilization might lead to serious consequences and comes with increased risk of susceptibility to cyber-attacks [3]. Because of variable data transmission media, specific services and complex network architecture, security functions should be considered with multiple layers in mind [4]. It is worth to take note that today's implementation of Smart Grids, because of its specific nature, might attract potential attackers for two reasons. Firstly, it is a critical network fitted with hundreds of devices operating based on the same principles. It allows for multiple reuse of broken security protocols and system vulnerabilities, which makes a potential attack all the more alluring. Secondly, a modern large network can be challenge potential attackers would like to undertake, e.g. to test their abilities. There is a reason IT network administrators are commonly convinced that there is no IT network no one would like to attack. To sum up, utilization of latest tele-information solutions is one of the most effective ways to assure increased effectiveness of electric power systems. It is especially important in heavily urbanized areas with relatively short distances between individual substations.

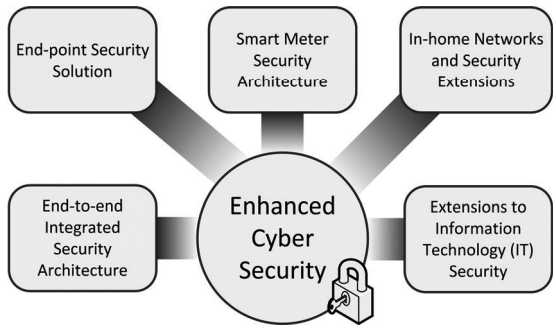

Fig. 1. A conceptual model of a smart grid security system components

Utilization of smart automated devices in networks with dense structures will allow for choosing the best from among available decisions, which can be hard to achieve in suburban and rural systems because of the lack of alternative routes or the need to disconnect large portions of networks. A quite important reason for which such a solution will be viable in the future only in the largest cities is protection of a large group of energy consumers situated within a relatively small area from consequences of a failure, where a long service downtime would entail serious consequences. It does not mean that energy consumers from suburban and rural areas should feel discriminated due to being deprived of such solutions. System distributors have prepared different energy provision solutions for them.

3. TASKS OF SMART AUTOMATION

Rapid development of electric power systems, in the perspective of their utilization in urban agglomerations, makes it so that security automation should be looked at not only in terms of security devices and intended functions, but of whole security systems. It is not always an easy task, especially from the perspective of possessed funding and expected security level. A properly designed security system will allow to react to not only all possible disturbances resulting from the nature of power electric system functionality, but also to intentionally initiated external incidents. Correctly and skillfully configured control and measurement devices can reliably take corrective action. The idea of such a solution is installation, within the network's structure, devices that will automatically communicate with each other and make the best decisions, adequate to a situation at hand. The most important function of smart security automation systems is automatically cutting off a compact line segment and restoring the rest of the system to the normal loss. In short, such devices must possess decision-making logic sufficiently complex to be able to take action in order to mitigate failure consequences in a relatively short time and based on information gathered from the immediate surroundings. Additional function of such a system is transfer and registration of all statistical information and event history to the SCADA operator. One should remember, however, that not even the most advanced logistical programs can ever replace a human, so the highest priority device in the system sends queries to the SCADA system and awaits the system operator's decision.

Electric power security automation can be divided into three groups: elimination automation, prevention automation and restitution automation. The goal of elimination automation is to prevent the spread of a failure's consequences by means of quick and selective elimination of damaged elements of the electric power system. Prevention automation performs an equally important task which is detecting and reporting potential threats and anomalies appearing during normal system operation. A threat might be both overloaded individual system elements and unbalanced active or reac-

tive power in the system. The third kind of automation is restitution automation the task of which is the fastest possible power provision to consumers after a damaged system fragment is shut down. The basic features of security automation are: reliability, selectivity, speed and sensitivity. Such a solution allows for relatively quick restoration of power, and the simple implementation, flexibility and ease of configuration due to decentralized automation allow for fast decision-making with no need for cooperation with SCADA/DMS systems. Smart automation devices can significantly decrease the time to restore power and energy availability in cable distribution networks. In case of a short circuit, they independently isolate one disturbed area and quickly restore power in the network areas unaffected by the short circuit (Fig. 2). The dispatcher is only informed about the short circuit or other system failure, but the automation systems do not await the operator's answer. Instead, they automatically communicate with each other in order to find the short-circuited area, isolate it and restore power in the network areas unaffected by the short circuit.

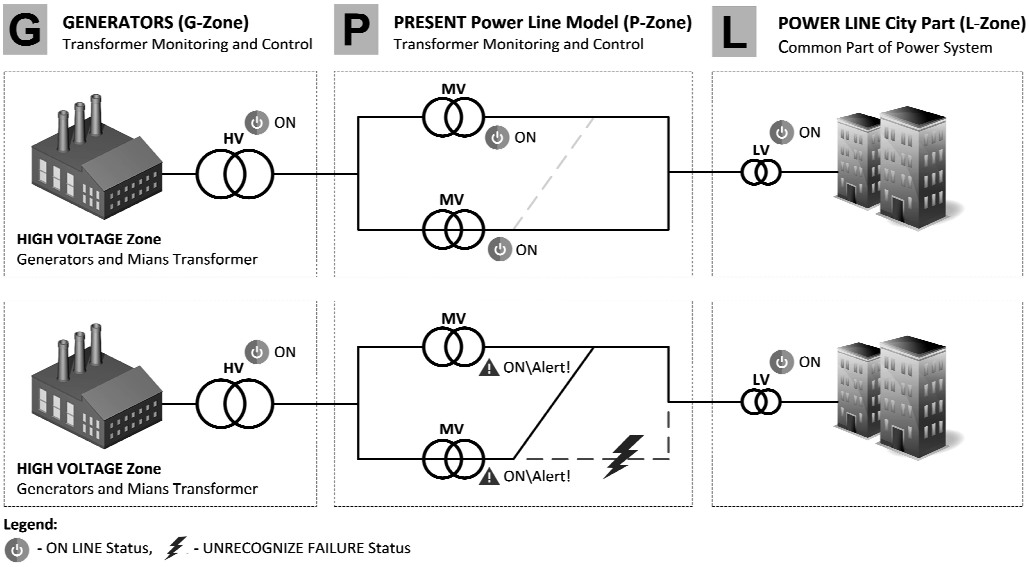

Fig. 2. Exemplary events in the form of short-circuited/damaged electric power lines

Another necessary element of modern electromagnetic systems is a central enterprise resource planning (ERP) system. Such a system, along with SCADA and control and measurement systems, is the basis of modern smart grid systems' functionality [5]. An electric power system's communication system is composed of a transmitter and a receiver, which is interchangeably in the form of security automation devices and communication channels. Utilized media type and network topology provide various levels of communication speed, security, reliability and resilience to external distur-

bances (Fig. 3). There are several types of communication media such as: radio systems, Ethernet, fiber optics, serial connectors or increasingly used communication by means of existing power lines – PLC (*Power Line Communication*). Each of the mentioned media has its own flaws and benefits, their utilization should take into account the potential effect and has to be adequate to specific cases.

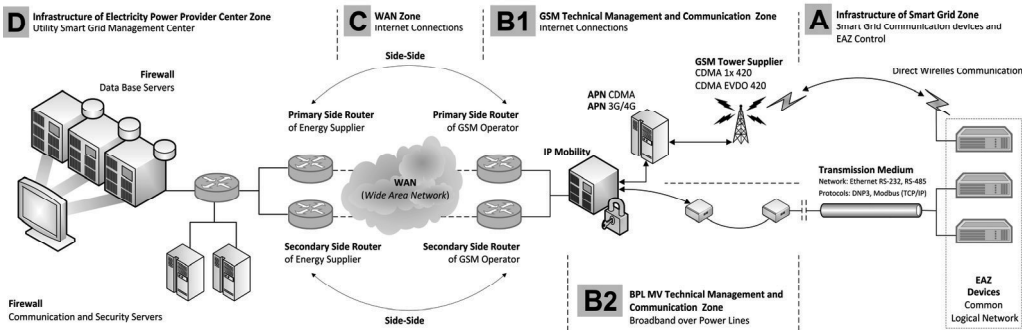

Fig. 3. A conceptual image of security automation communication within a Smart Grid

Communication protocols, being the basis for communication of all tele-information systems, are a collection of rules which allow different manufacturers' devices to communicate with each other. Communication protocols are responsible solely for establishing and controlling network communication, they also set the rules of data representation and are used for error detection and device authentication in tele-information networks. Communication protocols can be divided into two groups. The first one comprises of protocols based on physical protocols, and the second one – with layer protocols. Protocols based on physical protocols have been developed to ensure compatibility between devices offered by different producers, they allow for data transmission at a certain distance (not just locally). The electronics industry association (EIA) has developed universal protocols like RS232, RS422, RS423 and RS485 which are commonly utilized in data transmission. Moreover, these protocols, based on physical ones, are also included in the "physical layer" in the open system interconnection (OSI) model. Communication by means of layer protocols is also accounted for in the OSI model by the International Organization for Standardization (ISO).

All objects in a modern electric power network, from security automation devices to managed switches and routers, operate within a complicated communication structure, most commonly based on the TCP/IP protocol. Such a structure, or more precisely topology, is very varied: from simple serial communication protocols to advanced tele-information networks such as Ethernet networks or WWAN (*Wireless Wide Area Network*). Information exchange, depending on the degree of implementation of a device within the network, is performed on many levels of physical topology,

where each level can make use of different technologies (serial and Ethernet connections – MAN networks, fiber and wireless networks – WAN and WWAN). When talking about the issue of communication, one cannot forget the very important matter of security. Generally speaking, all technical means of detection and prevention of digital threats, ensuring security (of hardware and software), are tasked with protecting the operator's system from unauthorized access to the devices. It concerns all devices, not just at stations, but also in all network segments used by the operator. From the perspective of a potential intrusion, particularly dangerous processes are data transmission, modification or intentional destruction, or DoS (*Denial of Service*) attacks. It is especially important when networks aimed at control of automation devices go outside the physical boundaries of the operator-controlled area. So-called security procedures (security policy) are often omitted in discussions about security.

4. SMART ELECTRICAL POWER SYSTEMS' SECURITY

With the introduction of smart grids, the importance of assuring security for the energy sector grew due to rapid development of IT technologies and telecommunication infrastructures. That is why one should not forget about the security of IT system and information aimed at controlling increasingly varied control and measurement devices. Adequate protection should be considered as early as the design phase. Digital security must cover not only intentional attacks by e.g. disgruntled employees, corporate spies or terrorists, but also accidental endangerment of information infrastructure caused by human errors, equipment failures of natural disasters. Thus, created system vulnerabilities may allow the attacker to gain access into the network and control software and consequently to alter the network's load conditions in order to destabilize it.

Transformation of the current network structure into a smart grid necessitates a number of new security solutions borrowed from already utilized solutions, e.g. from baking systems or public administration. Typical problems of today's IT include hacking, data theft or even cyberterrorism, which will sooner or later also affect electric power grids. Implementation of smart grids by means of installation of remote reading meters, electronic network elements, construction of new IT systems with energy consumption data causes power engineers many entirely new security-related problems. A complex system of multilayered security requires an overall concept of ensuring information security.

Security in Smart Grid can be divided into three groups:

a) by the continuity and security of services:
   - ensuring continued electrical energy supply at a contractually guaranteed level, binding the supplier and customer (it also concerns cases of bidirectional energy transfer – smart grids with the participation of prosumer),

- ensuring confidentiality of information on clients and security of statistical data generated by them, such as "consumption amount", time of the greatest energy demand or its total absence,
- security related to energy distribution management process, and telemetry and personal data protection in datacenters;

b) by security class:
- protection from unauthorized access to digital data transmission media and physical security of devices in intermediate stations,
- protection of end-use telemetric devices from unauthorized access, transmission disruption or complete lock of their activities,
- analytical optimization models and decision-making processes;

c) by policy:
- data access policy – user authorization, permission management,
- management security policy – investment processes' principles and rules,
- system security policy – reaction to incidents, managing confidential information like passwords, cryptographic keys.

Migration of the current electric power grid model to that of a smart grid entails increasingly more direct investment of IT and telecommunication sectors. These sectors possess already existing cyber security standards that address system vulnerabilities, as well as software aimed at detection of known and potentially dangerous system vulnerabilities. The very same vulnerabilities should be assessed in the context of smart grid infrastructure. Moreover, smart grids will be characterized by additional weaknesses caused by their complexity, large number of shareholders and their operational requirements being time-sensitive.

Traditional understanding of cybersecurity assumes that it's a kind of protection that requires ensuring confidentiality, integrity and availability of an electronic information communication system. When discussing smart electric power grids, the definition of cybersecurity has to be made more extensive. Cybersecurity of smart grids encompasses both technologies and processes of energy systems and cybernetic systems, in operation and management of IT and power systems. These technologies and related processes assure security adequate to maintain confidentiality, integrity and availability of smart grid cybernetic infrastructure, like control systems, security, sensors and actuators.

The general strategy for smart grid security assumes both common requirements and specific ones for individual infrastructure portions. The main task of a cybersecurity strategy should be prevention. Nonetheless, reaction and restoration strategies should also be developed in case of a cybernetic attack on an electric power system.

Implementation of cybersecurity strategy requires definition and utilization of a general smart grid security risk assessment process. Risk is probability of an undesirable incident or event, as well as related consequences. This type of risk is a component of organizational risk. Organizational risk can entail many types of

risk (like investment, budgetary, program management, legal responsibility, security, inventory and information systems-related risks). The process of smart grid risk assessment is based on existing risk assessment means developed by the private and public sectors, and includes identification of consequences, susceptibility to attacks and threats in order to assess the smart grid-related risk. Because Smart Grids entail systems from the IT, telecommunication and energy sectors, the risk assessment process concerns all three sectors and their interaction with smart grids and smart metering.

Generally speaking, the priority goals of IT system security measures include confidentiality, integrity and availability. In industrial control systems, along with power systems, the security priorities are first availability, then integrity and confidentiality. Availability is the most important goal of cybersecurity.

Availability-related time delay in modern Smart Systems can be varied:

- 4 ms for protective relaying,
- sub-seconds for transmission wide-area situational structure monitoring,
- seconds for substation and feeder supervisory control and data acquisition (SCADA),
- minutes for monitoring non-critical equipment and some market pricing information,
- hours for meter reading and longer term market pricing information,
- days/weeks/months for collecting long-term data such as power quality information.

Integrity for power system operations includes assurance that:

- data has not been modified without authorization,
- source of data is authenticated,
- timestamp associated with the data is known and authenticated,
- quality of data is known and authenticated.

Confidentiality is the least critical for power system reliability. However, confidentiality is becoming more important, particularly with the increasing availability of customer information online:

- privacy of customer information,
- electric market information,
- general corporate information, such as payroll, internal strategic planning, etc.

In its broadest sense, cyber security for the power industry covers all issues involving automation and communications that affect the operation of electric power systems and the functioning of the utilities that manage them. This includes the goals of preventing, preparing for, protecting against, mitigating, responding to, and recovering from cyber events. In the power industry, the focus has been on implementing equipment that can improve power system reliability. Until recently, communications and IT equipment were typically seen as supporting power system

reliability. However, increasingly these sectors are becoming more critical to the reliability of the power system. One of the more interesting examples that could help to understand the importance of information transfer efficiency and security for proper electric power system functionality is the system failure from August 14, 2003. Initially small negligence by one of the system operators and the following unfortunate combination of events led to the biggest blackout in the history of the United States. The failure led to a shutdown of 265 power plants (531 power units) in the USA and Canada [6]. Interestingly enough, the on-going and cascading failures were primarily due to problems in providing the right information to the right place within the right time. Also, the IT infrastructure failures were not due to any terrorist or Internet hacker attack; the failures were caused by inadvertent events (mistakes), lack of key alarms, and poor design. Therefore, inadvertent compromises must also be addressed and the focus must be an all-hazards approach.

These hazard most commonly include:

- manmade deliberate threat – incidents that are either enabled or deliberately caused by human beings with malicious intent, e.g., disgruntled employees, hackers, nation-states, organized crime, terrorists, and industrial spies,
- manmade unintentional threat – focuses on incidents that are enabled or caused by human beings without malicious intent, e.g., careless users and operators/administrators that bypass the security controls,
- natural threat – focuses on non-manmade incidents caused by biological, geological, seismic, hydrologic, or meteorological conditions or processes in the natural environment, e.g., earthquakes, floods, fires, and hurricanes.

Providing energy by means of a smart grid includes flow of information allowing for continuous demand monitoring and demand control by means of influencing energy receivers. It will allow for flexible demand shaping and adjustment of supply to the daily demand. In combination with increasingly often utilized energy-efficient building solutions, devices and technological processes, it results in increased energy efficiency on a large scale and reduction of important risk factors – unstable energy balance and low energy efficiency.

Actions to be taken by 2030 for improvement of energy efficiency and development of competitive fuel and energy markets, provided for in the Polish Energy Policy, include particularly:

- implementation of demand side management techniques stimulated by daily variation of electric energy prices resulting from introduction of intraday market and transfer of price signals to receivers by means of electronic meters,
- abolition of limitations related to changing the provider by introduction of nation-wide norms concerning technical prices, installation and reading of electronic energy meters [7].

5. CONCLUSION

An important advantage of a Smart Power Grid is its ability to integrate with an existing energy system in order to intensify development of, among others, distributed generation, connection of renewable energy sources, introduction of energy storage systems and increase energy efficiency, and ultimately realization of the EU climate and energy package's goals [8]. Large-scale introduction of the Smart Grid will initiate changes in the current energy consumption patterns, both for individual (consumers and households) and collective (public utilities) entities. Despite many concerns about grid modernization, better and more directed grid management will contribute to its increased security, which will directly translate into cheaper exploitation and increased service quality.

ACKNOWLEDGMENTS

This paper was realized within NCBR project: ERA-NET, No. 1/SMARTGRIDS/2014, acronym SALVAGE "Cyber-Physical Security for the Low-Voltage Grids".

REFERENCES

[1] Dokumentacja techniczna Real VNC. Available in: https://www.realvnc.com/products/vnc/
[2] ZAKI M.J., jr., WAGNER M., *Data Mining and Analysis Fundamental Concepts and Algorithms*, Cambridge University Press, 2014.
[3] FLICK T., MOREHOUSE J., *Securing the Smart Grid. Next Generation Power Grid Security*, Elsevier, Inc., 2011.
[4] ANDERSON R.J., *Inżynieria zabezpieczeń. Bezpieczeństwo danych*, Wydawnictwo Naukowo-Techniczne, Warszawa 2005.
[5] Instytut Energetyki Instytut Badawczy, Instytut Energetyki/Badania/Elektroenergetyczna automatyka zabezpieczeniowa, 2012. Available in: https://www.ien.com.pl/consectetur
[6] OZAIST G., *Egipskie ciemności w USA*, Polska Energia, 2012, 5.
[7] Ministerstwo Gospodarki, *Polityka energetyczna Polski do 2030 roku. Załącznik do uchwały nr 202/2009 Rady Ministrów*, Dokument przyjęty przez Radę Ministrów w dniu 10 listopada 2009 r.
[8] Ministerstwo Środowiska, *Pakiet wyzwań – Polska wdraża pakiet klimatyczno-energetyczny. Podsumowanie*, Warszawa 2013.

composite load model, nonlinear optimization,
nonlinear least squares, genetic algorithms,
sequential quadratic programming

Paweł REGULSKI*

ESTIMATION OF COMPOSITE LOAD MODEL PARAMETERS AS A CONSTRAINED NONLINEAR PROBLEM

This paper presents the results of application of sequential quadratic programming to the estimation of the unknown composite load model parameters. Traditionally applied estimation methods, such as nonlinear least squares or genetic algorithms, suffer from a number of issues. Genetic algorithms exhibit premature convergence and require high computational resources and nonlinear least squares method is very sensitive to the initial guess and can diverge easily. This paper provides a comparison of all three methods based on computer-generated signals serving as field measurements. Accuracy and precision are assessed as well as computational requirements.

1. INTRODUCTION

Loads are one of the most uncertain elements of power systems. They play a key role in power system analysis and inaccurate modeling of loads may result in erroneous assessment of voltage stability [1], [2] as well as other types of studies, such as those on transient stability or load shedding [3], [4]. This becomes unacceptable in the current trend, where environmental considerations push the operating point of power systems closer to their stability limits.

Measurement-based load modeling [4], [5], in which the load characteristics are extracted through a parameter estimation procedure from appropriate field measurements, offers the means for obtaining accurate load models. In such an approach, the aim is to minimize the difference between the output of an assumed load model and the corresponding field measurements. The final reliability and accuracy of the load model relies heavily, among other things, on the selected parameter estimation technique, which is especially true in the case of a composite load (CL) model. The CL

* Wrocław University of Technology, Department of Electrical Power Engineering, Wybrzeże Wyspiańskiego 27, 50-370 Wrocław, Poland, email: pawel.regulski@pwr.edu.pl

model is a highly nonlinear model of an induction motor (IM) connected in parallel with a static load. It is used typically to model loads dominated by IMs, which may include not only industrial loads (large machines) but also residential and commercial loads (smaller, single-phase machines). Traditionally, methods such as nonlinear least squares (NLS) [6] or genetic algorithms (GA) [7] have been employed to solve the problem of finding the unknown load model parameter. However, these methods suffer from several flaws. NLS is prone to divergence and, as a deterministic method, is shows strong sensitivity to the initial guess. GA on the other hand, may exhibit premature convergence and it is more time-consuming then NLS. Moreover, both of the methods disregard the fact that the estimation of parameters of the CL model, from its definition, is a constrained problem. This paper addresses this particular issue by applying sequential quadratic programming (SQP) method, which is known to be efficient in solving problems of similar nature [8]. In the area of power systems it has been already successfully applied to solving the hydro unit commitment problem [9] as well as the optimal power flow problem [10].

2. COMPOSITE LOAD MODEL

The CL model is the most complex widely used load model and, according to a recent survey [11], about 30% of utilities around the world use it for dynamic power system studies. It is a voltage dependent model including a 3rd order IM model connected in parallel with a static load model. The IM model adopted in this work can be found in [5] and its full derivation is presented in [2]. The static part of the model is described by an exponential load (EL) model with the following equations:

$$P_S = P_{S0}\left(V/V_0\right)^{\alpha} \tag{1}$$

$$Q_S = Q_{S0}\left(V/V_0\right)^{\beta} \tag{2}$$

where V_0 is the pre-disturbance voltage in pu, P_{S0} and Q_{S0} are the pre-disturbance active and reactive power consumed by the static load, respectively, in W and var. P_S and Q_S are the static load power demands, respectively, in W and var, α and β are the static exponents and V is the actual rms voltage in pu.

The complete vector of unknown model parameters to be estimated is defined as follows:

$$\boldsymbol{\theta} = [H, R_s, X_s, R_r, X_r, X_m, A, B, K_P, T_0, \alpha, \beta] \tag{3}$$

where H is the inertia constant in s, R_s is the stator resistance in pu, X_s is the stator reactance in pu, R_r is the rotor resistance in pu, X_r is the rotor reactance in pu, $X_{m,}$ is the magnetizing reactance in pu, A and B are the torque coefficients and T_0 is the nominal torque at nominal speed in pu. The parameter K_P is defined as follows:

$$K_P = {P_{M0}}/{P_0} \tag{4}$$

where P_{M0} is the initial active power consumed by the IM, in W, and P_0 is the pre-disturbance active power measured at the load bus in W. Table 1 presents the searching space for the parameters defined in (3). It has been selected based on [1] and [2] to cover a wide range of types of motors and characteristics of static loads.

Table 1. Selected ranges of the CL model parameters

	Searching space	
	min	max
H	0.200	2.000
R_s	0.001	0.100
X_s	0.050	0.200
R_r	0.010	0.100
X_r	0.100	0.300
X_m	2.000	4.000
A	0.000	1.000
B	0.000	1.000
K_p	0.200	1.000
T_0	0.200	1.000
α	0.000	4.000
β	0.000	4.000

3. SEQUENTIAL QUADRATIC PROGRAMMING

The SQP approach has been extensively used in 1970s [12]. Its high efficiency and accuracy, when compared to other optimization methods, has been further proved by Schittkowski on a large number of test examples [13]. The SQP provides a framework for solving general nonlinear programming problems of the following form:

$$\min_{\mathbf{x}} f(\mathbf{x}) \tag{5a}$$

subject to

$$\begin{aligned} c_i(\mathbf{x}) &= 0, \qquad i \in \mathcal{E} \\ c_i(\mathbf{x}) &\geq 0, \qquad i \in \mathcal{I} \end{aligned} \tag{5b}$$

where $\mathbf{x} \in \mathbf{R}^n$, f is the objective function, c_i, $i \in \mathcal{E}$ are the equality constraints and c_i, $i \in \mathcal{I}$ are the inequality constraints.

The main concept behind the SQP approach is to model the problem (5) as a sequence of quadratic problems of the following form:

$$\min_{\mathbf{p}} f(\mathbf{x}_k) + \nabla f(\mathbf{x}_k)^T \mathbf{p} + \frac{1}{2} \mathbf{p}^T \nabla^2_{xx} \mathcal{L}_k \mathbf{p} \tag{6a}$$

subject to

$$\begin{aligned} \nabla c_i(x_k)^T \mathbf{p} + c_i(\mathbf{x}) &= 0, \qquad i \in \mathcal{E} \\ \nabla c_i(x_k)^T \mathbf{p} + c_i(\mathbf{x}) &\geq 0, \qquad i \in \mathcal{I} \end{aligned} \tag{6b}$$

where index k is the iteration number, $\mathbf{p}$ is the search direction in the quadratic problem, ∇ is the gradient operator and ∇^2_{xx} is the Hessian operator with respect to $\mathbf{x}$. The Lagrangian function $\mathcal{L}_k$ is described as follows:

$$\mathcal{L}_k = f(\mathbf{x}_k) - \boldsymbol{\lambda}_k^T c(\mathbf{x}_k) \tag{7}$$

where $\boldsymbol{\lambda}_k$ is a vector of Lagrange multipliers.

The quadratic problem (6) is solved using the *active set strategy*, which is an iterative approach. It starts with an initial guess of an active set $\mathcal{A}$, which for any feasible $\mathbf{x}$ is a set of the equality constraint indices $\mathcal{E}$ together with the indices of the inequality constraints for which $c_i(\mathbf{x}) = 0$:

$$\mathcal{A}(\mathbf{x}) = \mathcal{E} \cup \{ i \in \mathcal{I} \,|\, c_i(\mathbf{x}) = 0 \} \tag{8}$$

The *active set strategy* solves this equality constrained problem using the constraints, indices of which are included in the current active set $\mathcal{A}$. In each iteration it performs the following three major tasks:

a) it finds the direction towards the solution and calculates the length of the step,
b) it checks whether the step is violating any constrains, indices of which are not included in $\mathcal{A}$ and adds them to $\mathcal{A}$ if that is the case and
c) it removes the inequality constraint indices from $\mathcal{A}$ if the Lagrange multipliers corresponding to those constraints become negative, which suggests that the objective function can be further minimized by moving away from those constraints.

The above method terminates once the solution to the quadratic sub-problem is equal to 0 (the calculated direction increment at the current iteration is equal to 0) [8].

The final solution of the quadratic problem (6) is used to update the $\mathbf{x}_k$:

$$\mathbf{x}_{k+1} = \mathbf{x}_k + \alpha \mathbf{p} \tag{9}$$

where α is the step-length coefficient obtained using a line search approach to minimize a merit function, which ensures a sufficient decrease in the objective function [8]. After that, the iteration number k is incremented and a new quadratic problem is formulated. The procedure repeats until $\mathbf{x}_k$ meets the Karush–Kuhn–Tucker (KKT) optimality conditions [8].

The above paragraphs gave an introduction to what the sequential quadratic programing is. However, to implement it for solving the problem of estimation of unknown load model parameters, the suitable objective function of the problem must be defined. It must be followed with appropriate constraints.

For the CL model, the objective function for a given n samples of input data, i.e. measurements, can be defined as follows:

$$\min_{\boldsymbol{\theta}} \frac{1}{n} \sum_{k=1}^{n} [(P_{mk} - P_{CLMk}(\boldsymbol{\theta}))^2 + (Q_{mk} - Q_{CLMk}(\boldsymbol{\theta}))^2] \tag{10}$$

subject to the bound constraints defined in Table 1 and the inequality $A + B \leq 1$ imposed on the torque coefficients [5]. P_{mk} and Q_{mk} are the k-th sample of measured active and reactive powers, respectively, in W and var and P_{CLMk} and Q_{CLMk} are the k-th sample of estimated active and reactive powers, respectively, in W and var.

4. RESULTS

SQP has been tested and compared against the traditional methods (NLS and GA) in a series of computer simulations. Firstly, 6 test voltage signals have been generated

to excite the CL model. These include step changes and ramps of different magnitudes and are depicted in Figure 1.

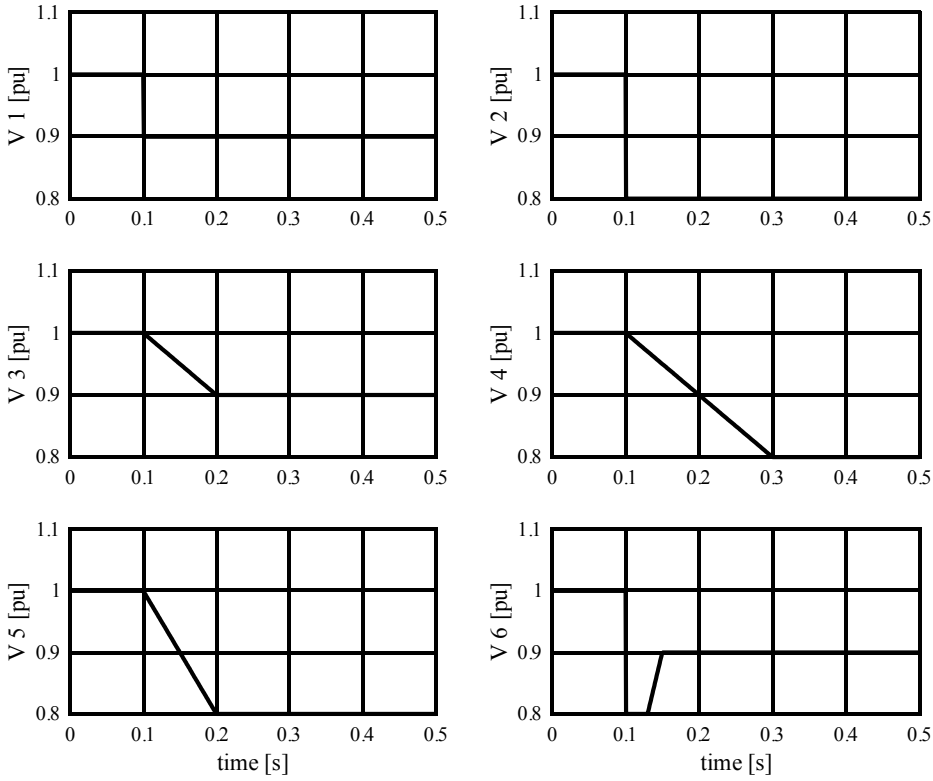

Fig. 1. Voltage signals used to excite the CL model

Based on the 6 generated voltage signals, active and reactive power responses of the CL model were simulated for a given set of parameters. These responses are depicted in Figure 2. Such a set of computer-generated signals was assumed as field measurements for the purpose of the estimation process.

Initial conditions for each method were obtained from the same set of 100 parameter vectors randomly generated from the assumed searching space (Table 1). In the case of SQP and NLS, each vector was used as a starting point of the procedure, for a total of 100 runs for each method. On the other hand, GA uses the whole set of vectors as an initial population. However, due to the nature of the method, which is driven to an extent by random processes, the estimation procedure has been repeated 100 times to assess its average performance. In this way, each method returned 100 solutions, which allowed for a reasonable comparison.

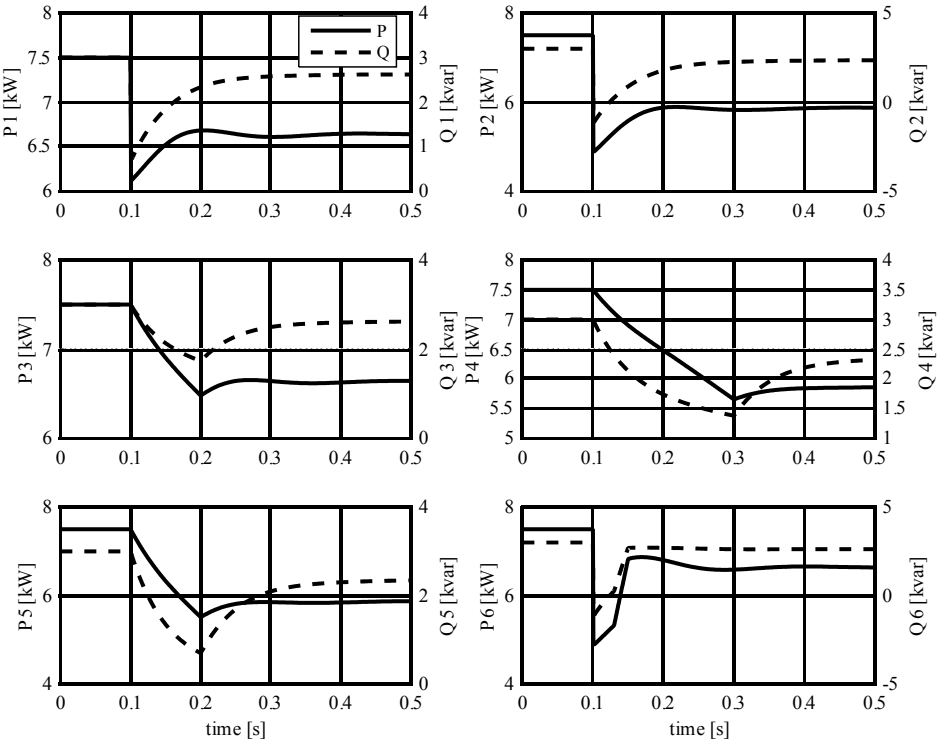

Fig. 2. Active and reactive power responses of the assumed CL model

In the estimation process, 2 out of 6 data sets have been used. That includes measurement 2 (voltage step change) and measurement 4 (voltage ramp). This allows covering a wider range of the model's responses and improves the generality of the identified parameters. It is important to notice that using insufficient amount of data at the training stage may result in loss of generality (overtraining), which manifests itself in a very good fit at the training stage and a poor fit at the validation stage. In this case, the estimation result has been validated against all 6 data sets (cases) and the results have been presented in Tables 2 and 3. Firstly, it can be observed that SQP achieves the smallest average relative errors in 100 trials and NLS achieves the highest (Table 2). Secondly, standard deviation of the relative errors presented in Table 2 shows that SQP is also the most consistent method, which makes it more accurate and precise than the other two approaches. The results also confirm that NLS is very sensitive to the initial guess and can easily diverge. Figure 3 depicts comparison of all 3 methods in their best trial. It can be concluded that NLS can achieve accuracy similar to that of SQP, but only if the initial guess is appropriately selected.

Table 2. Average relative errors obtained for each case (based on 100 trials)

	GA		NLS		SQP	
	Perr [%]	Qerr [%]	Perr [%]	Qerr [%]	Perr [%]	Qerr [%]
Case 1	0,163	0,645	2,042	7,803	0,009	0,081
Case 2	0,240	1,234	2,813	18,919	0,008	0,057
Case 3	0,139	0,489	1,810	7,012	0,006	0,065
Case 4	0,136	0,628	1,988	12,018	0,006	0,038
Case 5	0,185	0,949	2,370	15,905	0,007	0,041
Case 6	0,195	0,784	2,448	9,179	0,011	0,092

Table 3. Standard deviation of the relative errors obtained for each case (based on 100 trials)

	GA		NLS		SQP	
	Std. Perr	Std. Qerr	Std. Perr	Std. Qerr	Std. Perr	Std. Qerr
Case 1	0,237	0,420	3,064	14,079	0,010	0,047
Case 2	0,363	1,245	3,744	36,769	0,014	0,086
Case 3	0,170	0,356	3,011	13,780	0,009	0,038
Case 4	0,155	0,824	2,815	23,531	0,009	0,066
Case 5	0,254	1,096	3,212	31,190	0,010	0,079
Case 6	0,320	0,486	3,293	16,596	0,014	0,053

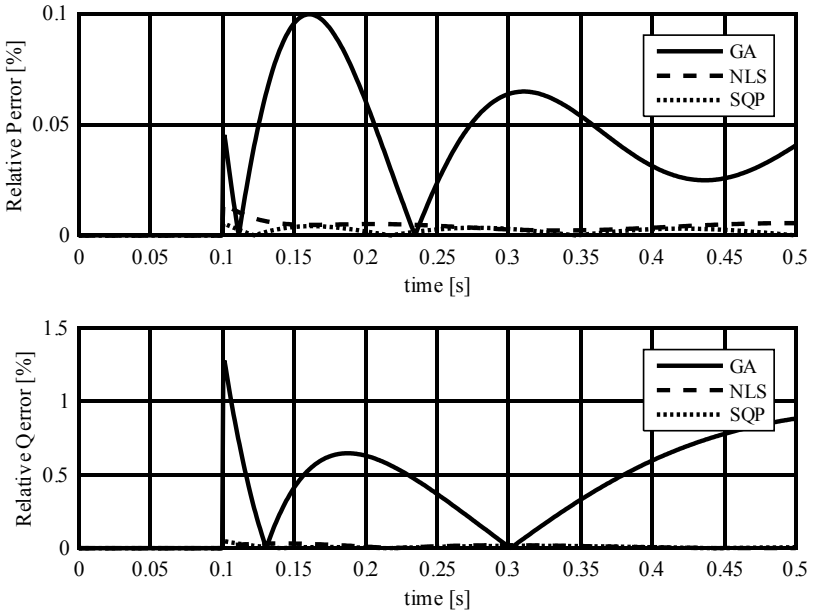

Fig. 3. Comparison of best estimations achieved by each method (validation using case 2)

The selection of the training set in this particular case turned out to be successful. There are no obvious discrepancies between average relative errors obtained for training cases and validation cases (Table 2). Other combinations of cases forming the training set have been tested with very similar results. It has been also observed that voltage step changes reveal more dynamic properties than voltage ramps and it advisable always to include a voltage step change in the training set for more reliable results.

In terms of computational performance, the average execution times for each method are presented in Table 4. In this particular test, SQP is over two times slower than NLS, but still much faster than GA. It should also be noted that the implementation of GA, in this case, takes advantage of parallel computing and it utilizes 4 available cores of the CPU. On a single-core CPU the average execution time of GA would be approximately 4 times higher.

Table 4. Average execution times in seconds
(based on 100 trials)

GA	NLS	SQP
184	9	23

5. CONCLUSIONS

This paper proposed the application of SQP to estimate the unknown parameters of the CL model from field measurements. This method takes into account constrains, which was impossible with the use of traditional methods such as NLS or GA. SQP achieves highest accuracy and precision without the loss of the generality of the assumed load model. Its execution time, although higher than that of NLS, still allows for online load monitoring with the assumption that appropriate voltage disturbances do not occur too often.

The execution time of SQP, when compared to NLS, reflects its more complex implementation, which might be recognized as a disadvantage. However, the benefits of this approach outweigh this flaw significantly.

The preliminary tests presented in this paper have provided very promising results. In the next step, SQP should be examined using either laboratory or field measurements to ensure that the benefits of using SQP can also be achieved in practice.

REFERENCES

[1] VAN CUTSEM T., VOURNAS C., *Voltage Stability of Electrical Power System*, Kluwer Academic Publishers, 1998.
[2] KUNDUR P., *Power System Stability and Control*, McGraw-Hill, 1994.

[3] RIFAAT R.M., *On Composite Load Modeling for Voltage Stability and Under Voltage Load Shedding*, Power Engineering Society General Meeting, 2004, IEEE, June 2004, Vol. 2, pp. 1603–1610.
[4] JU P., WU F., SHAO Z.-Y., ZHANG X.-P., FU H.-J., ZHANG P.-F., HE N.-Q., HAN J.-D., *Composite Load Models Based on Field Measurements and Their Application in Dynamic Analysis*, Generation, Transmission and Distribution, IET, Sept. 2007, Vol. 1, No. 5, pp. 724–730.
[5] MA J., DONG Z.-Y., HE R.-M., HILL D.J., *Measurement-based Load Modeling using Genetic Algorithms*, IEEE Congress on Evolutionary Computation 2007. CEC 2007, Sept. 2007, 25–28, pp. 2909– 2916.
[6] WANG J.-C., CHIANG H.-D., CHANG C.-L., LIU A.-H., HUANG C.-H., HUANG C.-Y., *Development of a frequency-dependent composite load model using the measurement approach*, IEEE Transactions on Power Systems, Aug. 1994, Vol. 9, No. 3, pp. 1546–1556.
[7] WEN J.Y., JIANG L., WU Q.H., CHENG S.J., *Power System Load Modeling by Learning Based on System Measurements*, IEEE Transactions on Power Delivery, April 2003, Vol. 18, No. 2, pp. 364–371.
[8] NOCEDAL J., WRIGHT S. J., *Numerical Optimization*, 2nd Ed., Springer, 2006.
[9] FINARDI E.C., DA SILVA E.L., *Solving the hydro unit commitment problem via dual decomposition and sequential quadratic programming*, IEEE Transactions on Power Systems, May 2006, Vol. 21, No. 2, pp. 835–844.
[10] SIVASUBRAMANI S., SWARUP K.S., *Sequential quadratic programming based differential evolution algorithm for optimal power flow problem*, Generation, Transmission and Distribution, IET, Nov. 2011, Vol. 5, No. 11, pp. 1149, 1154.
[11] MILANOVIC J.V., YAMASHITA K., MARTINEZ VILLANUEVA S., DJOKIC S.Z., KORUNOVIC L.M., *International Industry Practice on Power System Load Modeling*, IEEE Transactions on Power Systems, Aug. 2013, Vol. 28, No. 3, pp. 3038–3046.
[12] BIGGS M.C., *Constrained Minimization Using Recursive Quadratic Programming*, Towards Global Optimization, North-Holland 1975, pp. 341–349.
[13] HOCK W., SCHITTKOWSKI K., *Test Examples for Nonlinear Programming Codes*, Lecture Notes in Economics and Mathematical Systems, Vol. 187, Springer, 1981.

capacitive voltage transformer,
ferroresonance, suppression circuit,
chaotic behaviour, simulation

Jan IŻYKOWSKI*
Eugeniusz ROSOŁOWSKI*
Piotr PIERZ*

ANALYSIS OF FERRORESONANCE OSCILLATIONS IN CAPACITIVE VOLTAGE TRANSFORMER

Analysis of ferroresonance oscillations in capacitive voltage transformer is presented. For this purpose an analytical approach to ferroresonance is firstly introduced. With use of the harmonic balance method the condition for avoiding stable subharmonic oscillations of the 3rd mode is stated. In the next step the ATP-EMTP simulation based investigations are carried out to find the suppression circuit parameter (or parameters) which assure damping of the nonlinear oscillations in accordance to the requirements of the standards. Two kinds of suppression circuits designed for the considered capacitive voltage transformer construction are investigated. The possible chaotic phenomena resulting from nonlinear oscillations are also examined. The obtained results are presented and discussed.

1. INTRODUCTION

The predominant sources of voltage signals for protective, monitoring, measuring and control devices in high voltage (HV) and extra high voltage (EHV) systems are capacitive voltage transformers (CVTs) which are also named as coupling capacitor voltage transformers (CCVTs) [1]. A CVT provides a cost-effective way of obtaining a secondary voltage for HV and EHV systems [1], [2]. Its functional scheme [1]–[4] is depicted in Fig. 1. A CVT is composed of a capacitive voltage divider (C_1 and C_2 – both consisting of some capacitor elements connected in series), a compensating reactor (L_{CR}) and a step-down inductive voltage transformer (Tr) usually with two secondary windings. In the scheme of Fig. 1, besides the primary voltage (u_p) and

* Department of Electrical Power Engineering, Wrocław University of Technology, Wrocław, Poland.

secondary voltages (u_{s1}, u_{s2}) one also distinguishes the intermediate voltage (u_i), which is usually at the level of around 20 kV.

Two kinds of CVT transient conditions are taken for analysis which is aimed at evaluation of CVT transient performance:

- non-linear oscillations under saturation of a magnetic core of a CVT step-down inductive voltage transformer (Tr in Fig. 1) [1]–[9],
- discharging of a CVT internal energy during decreasing the primary voltage (u_p) which is the case of short circuits on the associated transmission line [10]–[14].

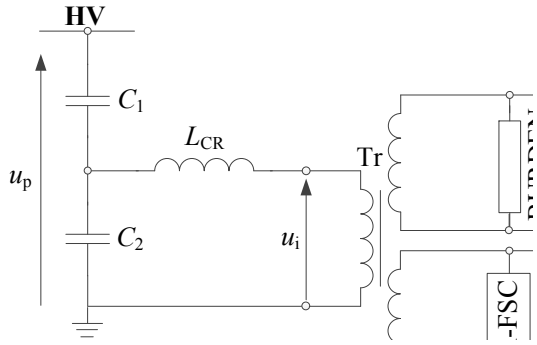

Fig. 1. Schematic diagram of CVT: C_1, C_2 – stack capacitors; L_{CR} – compensating reactor; Tr – inductive step-down transformer; A-FSC – anti-ferroresonance suppressing circuit; BURDEN – burden imposed by connected protective and other devices

Non-linear oscillations can appear when the operating point of the magnetizing characteristic of the step-down transformer is shifted to the saturation region. The energy stored in the capacitive and inductive elements of the device generate transients with low frequency of aperiodic character which could last of long period. On the other hand a sudden change of voltage at the primary terminals of the step-down transformer could cause saturation of the magnetic core what with interaction with capacitance are sources of non-linear oscillations called ferroresonance. CVTs are therefore equipped with special anti-ferroresonance circuit (A-FSC in Fig. 1) for avoiding stabilization of the sub-harmonics and also assuring adequately fast damping of the oscillations. Both, passive [3]–[7] and active [8] suppression circuits are used. Power electronic elements are utilized for constructing the active circuits [8].

In turn, the CVT generated transients under short circuits on the associated transmission line are simpler for analysis since a CVT still operates at its linear range [10]–[14]. Such transients are commonly investigated in relation to their influence of protective relays operation. This issue is out of the scope of this paper.

2. SUBHARMONIC FERRORESONANCE IN CVTS

2.1. INTRODUCTION

CVTs installed in a power system operate during normal steady state conditions within a linear range for a step-down transformer (Fig. 1). However, under some disturbances this is not so. The exploitation experiences and laboratory tests show that extensive nonlinear oscillations can be generated in the CVT circuit. Such oscillations can appear under the disturbances such as [5], [10]:

- interruption of the short-circuit in the secondary CVT winding when the protecting fuse gets blown out,
- interruption of the short-circuit at the stack capacitor C_2 due to operation of the spark gap which protects it (the spark gap is not shown in Fig. 1),
- sudden appearing of the CVT primary voltage under switching on or interruption of the short-circuit at the CVT primary side,
- increase of the CVT primary voltage due to overvoltage,
- lightning-caused ferroresonance.

2.2. DESIGN OF FERRORESONANCE SUPPRESSION CIRCUIT

The exploitation experiences and laboratory tests show that if a CVT is not equipped with a properly designed suppression circuit, the subharmonic ferroresonance phenomenon [3]–[8] can occur. Subharmonic oscillations of 3rd or 5th mode can be generated in a CVT circuit. This is also known that more severe conditions are for damping the 3rd subharmonic oscillations and thus this will be concerned further. It is desired to prevent stabilization of such subharmonics and moreover to assure their fast damping, accordingly to the requirements imposed by the international standards [9]. To achieve this goal, a special anti-ferroresonance suppression circuit has to be applied at the step-down transformer output. In Fig. 1 it is presented that such circuit is connected to the dedicated winding, i.e. separately from the burden.

As so far, there are no design methods with the calculation procedure for selecting the suppression circuit parameter (or parameters). This is so since the CVT circuit has to be considered as a non-linear circuit. This paper is aimed at providing the design method for the suppression circuit which is based on the 2-step procedure:

- preliminary selection of the circuit parameters which assure that presence of stable subharmonic oscillations of 3rd mode are not possible,
- tuning the circuit parameters which assure that the standard requirements are satisfied with the aid of digital simulation.

Knowledge of the border conditions for avoiding stable subharmonics (1st step) facilitates carrying out the 2nd step of the design.

2.3. ANALYTICAL APPROACH TO SUBHARMONIC FERRORESONANCE

Since the CVT circuit is considered as a non-linear circuit its analytical analysis limits to the steady state considerations. For this purpose the harmonic balance method [10] will be utilized. This method assumes that the steady state solution for the nonlinear circuit can be represented by a linear combination of sinusoids, then balances current and voltage sinusoids to satisfy Kirchhoff's law.

An equivalent circuit diagram of a CVT used for the harmonic balanced method in relation to the subharmonic 3rd mode is presented in Fig. 2.

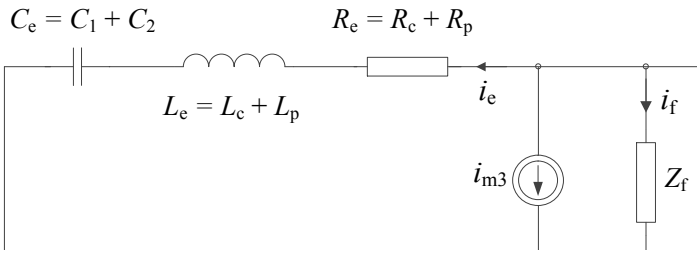

Fig. 2. Equivalent circuit diagram of CVT for studying 3rd subharmonic ferroresonance with all parameters related to the primary side of the step-down transformer: C_e – equivalent capacitance of capacitive divider, L_e – sum of inductances of the compensating reactor and of the primary winding of the step-down transformer, R_e – analogously as L_e, i_{m3} – current source of the 3rd harmonic current, Z_f – ferroresonance suppression circuit, Z_b – burden

In analytical considerations the following polynomial approximation of a magnetizing characteristic (magnetizing current i_m as a function of linkage flux ψ) is commonly used:

$$i_m = \sum_{k=0}^{n} a_{2k+1} \psi^{2k+1} \tag{1}$$

The number of terms used in (1) is: $n + 1$ and, in general, if the higher order approximation (i.e. higher n) is used, a better accuracy is achieved. However, this results in more complex analytical analysis or even in no possibility to obtain the solution without involving numerical calculation algorithms. This is the case also for analytical considerations of subharmonic ferroresonance in CVTs dealt in this paper. Therefore, it appears that a reasonable analytical approach can be carried out with using the following 3rd order ($n = 1$) approximation of the magnetizing characteristic:

$$i_m = a_1 \psi + a_3 \psi^3 \tag{2}$$

Limiting the presence of the fundamental frequency and the subharmonic 3rd mode in the CVT circuit, the linkage flux of the step-down transformer can be expressed as:

$$\psi(t) = \Psi_1 \cos(\omega t + \varphi) + \Psi_3 \cos\left(\frac{\omega t}{3}\right) \tag{3}$$

where the unknowns are: Ψ_1, Ψ_3 – magnitudes of the linkage flux for the fundamental frequency and 3rd subharmonic, respectively; φ is the phase displacement.

Substituting (3) into (2) and expanding the products of cosine functions into their sums one obtains the magnetizing current in the following form:

$$\begin{aligned} i_{\mathrm{m}} = {} & F_1 \cos\left(\frac{\omega t}{3}\right) + F_2 \cos\left(\frac{\omega t}{3} + \varphi\right) + F_3 \cos(\omega t) \\ & + F_4 \cos(\omega t + \varphi) + F_5 \cos\left(\frac{5\omega t}{3} + \varphi\right) + F_6 \cos\left(\frac{5\omega t}{3} + 2\varphi\right) \\ & + F_7 \cos\left(\frac{7\omega t}{3} + 2\varphi\right) + F_8 \cos(3\omega t + 3\varphi) \end{aligned} \tag{4}$$

where:

$$F_1 = a_1\Psi_3 + \frac{3}{2}a_3\Psi_1{}^2\Psi_3 + \frac{3}{4}a_3\Psi_3{}^2, \quad F_2 = \frac{3}{4}a_3\Psi_1\Psi_3{}^2,$$

$$F_3 = \frac{1}{4}a_3\Psi_1\Psi_3{}^2, \quad F_4 = a_1\Psi_1 + \frac{3}{4}a_3\Psi_1{}^3 + \frac{3}{2}a_3\Psi_1\Psi_3{}^2,$$

$$F_5 = \frac{3}{4}a_3\Psi_1\Psi_3{}^2, \quad F_6 = \frac{3}{4}a_3\Psi_1{}^2\Psi_3,$$

$$F_7 = \frac{3}{4}a_3\Psi_1{}^2\Psi_3, \quad F_8 = \frac{1}{4}a_3\Psi_1{}^3.$$

The 3rd subharmonic of the magnetizing current (4) taken for further analysis is thus equal:

$$i_{\mathrm{m3}}(t) = F_1 \cos\left(\frac{\omega t}{3}\right) + F_2 \cos\left(\frac{\omega t}{3} + \varphi\right) \tag{5}$$

Since the 3rd subharmonic of the linkage flux (3) is being assumed as:

$$\psi_3(t) = \Psi_3 \cos\left(\frac{\omega t}{3}\right) \tag{6}$$

the 3rd subharmonic of the voltage drop across the magnetizing branch equals:

$$u_3(t) = \frac{\mathrm{d}\psi_3(t)}{\mathrm{d}t} = -\frac{\omega}{3}\Psi_3 \sin\left(\frac{\omega t}{3}\right) \tag{7}$$

Applying the complex number analysis for the 3rd subharmonic to the CVT equivalent circuit (Fig. 2) one obtains:

$$\underline{I}_{\mathrm{m3}} = -\underline{Y}_3 \underline{U}_3 \tag{8}$$

The admittance $\underline{Y}_3$ for the 3rd subharmonic from (8) is determined by the parameters of three branches which are in parallel to the magnetizing branch (Fig. 2):

$$\underline{Y}_3 = \frac{1}{\dfrac{3}{\mathrm{j}\omega C_\mathrm{e}} + \mathrm{j}\dfrac{\omega}{3} L_\mathrm{e} + R_\mathrm{e}} + \frac{1}{Z_\mathrm{f}\left(\mathrm{j}\dfrac{\omega}{3}\right)} + \frac{1}{Z_\mathrm{b}\left(\mathrm{j}\dfrac{\omega}{3}\right)} \tag{9}$$

Rewriting (8) with use of (5) and (7) yields the following complex number equation:

$$\Psi_3\left(a_1 + \frac{3}{2}a_3\Psi_1^{\,2} + \frac{3}{4}a_3\Psi_3^{\,2} + \frac{3}{4}a_3\Psi_1\Psi_3 \mathrm{e}^{\mathrm{j}\varphi}\right) = -\mathrm{j}\underline{Y}_3 \frac{\omega}{3}\Psi_3 \tag{10}$$

Resolving (10) into the real and imaginary parts one obtains the following set of two equations:

$$\begin{aligned} \frac{3}{4}a_3\Psi_1\Psi_3\cos(\varphi) &= -\frac{\omega}{3}\,\mathrm{real}(\mathrm{j}\underline{Y}_3) - a_1 - \frac{3}{2}a_3\Psi_1^{\,2} - \frac{3}{4}a_3\Psi_3^{\,2} \\ \frac{3}{4}a_3\Psi_1\Psi_3\sin(\varphi) &= -\frac{\omega}{3}\,\mathrm{imag}(\mathrm{j}\underline{Y}_3) \end{aligned} \tag{11}$$

After determining $\cos(\varphi)$ and $\sin(\varphi)$ from (11) and utilizing Pythagorean trigonometric identity, after performing tedious derivations, one obtains the following equation for the sought magnitude of the 3rd subharmonic of the linkage flux:

$$\left(\frac{9}{16}a_3^{\,2}\right)\Psi_3^{\,4} + \left(\frac{3}{2}Ma_3 - \frac{9}{16}a_3^{\,2}\Psi_1^{\,2}\right)\Psi_3^{\,2} + \left(M^2 + N^2\right) = 0 \tag{12}$$

where for the purpose of the formula shortening the following quantities have been introduced:

$$\begin{aligned} M &= \frac{\omega}{3}\,\mathrm{real}(\mathrm{j}\underline{Y}_3) - a_1 - \frac{3}{2}a_3\Psi_1^{\,2} \\ N &= \frac{\omega}{3}\,\mathrm{imag}(\mathrm{j}\underline{Y}_3) \end{aligned} \tag{13}$$

Two solutions (marked with the subscripts 1 and 2) of (12) for the magnitude of the 3rd subharmonic of the linkage flux squared (Ψ_2^3) are:

$$(\Psi_2^3)_{1,2} = \frac{1}{2}\Psi_1^2 - \frac{4}{3}\frac{M}{a_3} \pm \sqrt{\Delta_1} = 0 \tag{14}$$

where the determinant Δ_1 is expressed:

$$\Delta_1 = \frac{1}{4}\Psi_1^4 - \frac{4}{3}\frac{M}{a_3}\Psi_1^2 - \frac{16}{9}\frac{N^2}{a_3^2} \tag{15}$$

The stable 3rd subharmonic oscillations are not possible to occur if the solutions (14) are not being real numbers. This is the case if the determinant (15) is negative:

$$\Delta_1 = \frac{1}{4}\Psi_1^4 - \frac{4}{3}\frac{M}{a_3}\Psi_1^2 - \frac{16}{9}\frac{N^2}{a_3^2} < 0 \tag{16}$$

In order to determine the quantities M, N, defined in (13), which are involved in the inequality (16), it is taken into account that:

$$\begin{aligned} \text{real}(\text{j}\underline{Y}_3) &= -\text{imag}(\underline{Y}_3) \\ \text{imag}(\text{j}\underline{Y}_3) &= \text{real}(\underline{Y}_3) \end{aligned} \tag{17}$$

As a result, the quantities M, N are as follows:

$$\begin{aligned} M &= \frac{\omega}{3}\text{imag}(\underline{Y}_3) - a_1 - \frac{3}{2}a_3\Psi_1^2 \\ N &= -\frac{\omega}{3}\text{real}(\underline{Y}_3) \end{aligned} \tag{18}$$

Substitution of (18) into (16) results in the following inequality for the condition that stable 3rd subharmonic oscillations are not possible to occur:

$$\frac{7}{4}\Psi_1^4 - \frac{4}{3a_3}\left(\frac{\omega}{3}\text{imag}(\underline{Y}_3) - a_1\right)\Psi_1^2 + \frac{16}{9a_3^2}\left(\frac{\omega}{3}\text{real}(\underline{Y}_3)\right)^2 > 0 \tag{19}$$

There are the following possibilities for generating stable 3rd subharmonic oscillations, namely the parameters of the CVT linear parameters {real ($\underline{Y}_3$), imag($\underline{Y}_3$) and the coefficient a_1 used for the nonlinear characteristic approximation (2)} are such that:

- stable subharmonic oscillations are not possible to occur if the determinant (Δ_2) for the double quadratic polynomial at the left side of (19) is negative, i.e.:

$$\Delta_2 = \left(\frac{\omega}{3}\,\mathrm{imag}(\underline{Y}_3) - a_1\right)^2 - 7\left(\frac{\omega}{3}\,\mathrm{real}(\underline{Y}_3)\right)^2 < 0 \tag{20}$$

or in a compact form:

$$\mathrm{real}(\underline{Y}_3) > \frac{1}{\sqrt{7}}\left(\mathrm{imag}(\underline{Y}_3) - \frac{3a_1}{\omega}\right) \tag{21}$$

- stable subharmonic oscillations are possible to occur if the condition (21) is not satisfied, however, only if the CVT is supplied with the voltage such that the magnitude of the fundamental frequency flux linkage (Ψ_1) is from the range:

$$(\Psi_1)_1 < \Psi_1 < (\Psi_1)_2 \tag{22}$$

where: $(\Psi_1)_1$, $(\Psi_1)_2$ are two solutions of the equation obtained by comparing the left side of (16) with zero.

This is worth to mention that in case of satisfying (22) the stable 3rd order subharmonic oscillations can be generated or not. This depends on the kind of disturbance initiating the transients. This is difficult to determine analytically which disturbance will lead to generating subharmonic oscillations and which disturbance will not initiate the subharmonic ferroresonance. However, this can be checked in a simulative way.

3. QUANTITATIVE ANALYSIS OF SUBHARMONIC FERRORESONANCE IN CVT

3.1. ANALYZED CVT CONSTRUCTION

Real, existing construction of CVTs which are installed at 220 kV transmission lines in Poland is taken for quantitative analysis of subharmonic ferroresonance. Magnetizing characteristic of the step-down transformer, related to its primary side (i.e. at the intermediate voltage (u_i) level), is presented in Fig. 3. This characteristic has been approximated by the formula (1) using weighted least error square method. Assuming $n = 1$ in (1) and taking small weights for high magnetizing current we can obtain the approximation coefficients: $a_1 = 13.85\text{e}{-6}$, $a_3 = 85.9\text{e}{-10}$.

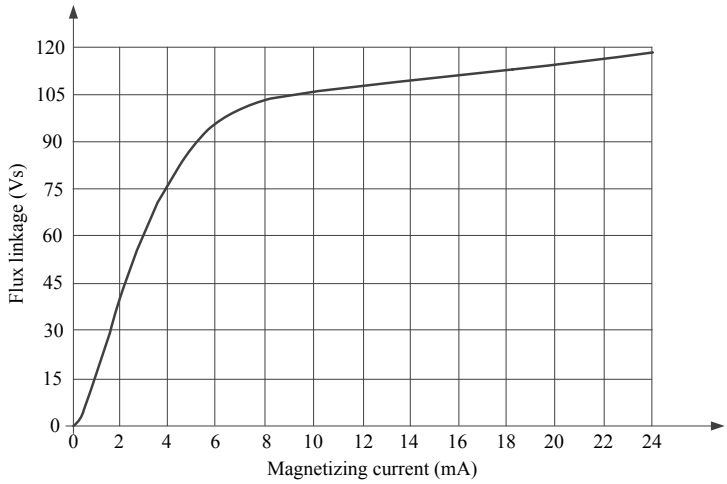

Fig. 3. Magnetizing characteristic of the step-down transformer

The other basic parameters, related to the equivalent circuit diagram from Fig. 2, are as follows: C_1 = 4.974 nF, C_2 = 47.160 nF (thus the equivalent capacitance of the capacitor divider: C_e = 52.135 nF), L_e = 194.81 H, R_e = 7242.0 Ω, L_b = 0.32 H, R_b = 133.04 Ω (including secondary side parameters of the transformer). The step-down transformer is $21000/\sqrt{3}$ V / $100/\sqrt{3}$ V / $100/\sqrt{3}$ V. The rated burden is 150 VA, however, for testing the speed of damping nonlinear oscillations according to the Polish standard [9], which is compatible with European standards, it is considered that the CVT under the test is lightly loaded with the maximal load of 5 VA. This imposes more severe conditions for damping nonlinear oscillations. According to the standard [9] the test is conducted by opening the secondary winding of the step-down transformer, which was previously short circuited. Such the test relies thus on charging of the CVT circuit with large amount of energy during the secondary winding short circuited and then by opening the winding intensive transients are occurring. This can shift the operation point on the magnetizing characteristic of the step-down transformer to its non-linear region. Damping of non-linear oscillations during such the test is considered as effective if their influence on magnitude of the CVT secondary voltage after 10 cycles (200 ms for 50 Hz fundamental frequency) from interrupting the short circuited winding is not greater than 10%. The other test details are specified in the standard [9].

Initially it is taken that the analysed CVT is equipped, as presently, with anti-ferroresonance suppression resistance (R_f) – Fig. 4a. Then it is considered that this resistance is to be replaced by the $R_fL_fC_f$ circuit with the parameters L_f, C_f tuned at the fundamental frequency resonance, thus not consuming active power during fundamental frequency steady state.

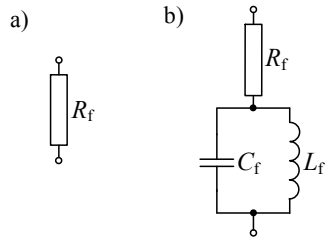

Fig. 4. Considered suppression circuits: a) suppression resistance, b) suppression circuit not consuming active power at fundamental frequency

The design of the suppression circuits is carried out with use of the 2-step procedure proposed in this paper. In the first step, the introduced analytical approach to 3rd subharmonic ferroresonance is applied for preliminary selection of the suppression circuit parameter (parameters). Then, the final selection is carried out with use of the ATP-EMTP simulation [15] for assuring that the requirements of the standard [9] are satisfied. For modelling a considered CVT construction (Fig. 1), which are manufactured as single phase units, a three-winding transformer model of the ATP-EMTP program [15] with including nonlinear magnetizing characteristic has been utilized for modelling the step-down transformer. The other elements of the CVT were modelled as *RLC* branches (Fig. 5).

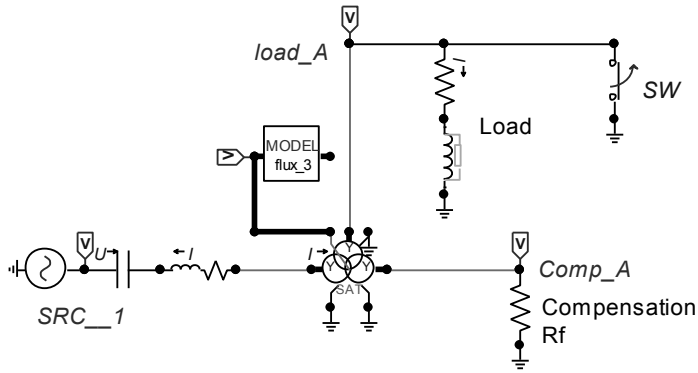

Fig. 5. ATP-EMTP model for simulation of CVT scheme

The step-down transformer is represented by the standard 3-phase 3-winding Y/y/y transformer model where only one phase (phase A) is utilized. The transformer flux linkage is calculated by integration of a magnetizing voltage in MODELS block *flux_3*. The switch SW is applied to introduce the oscillations: after being closed it is then forced to open.

Main advantage of the proposed design procedure is that having the preliminary selection from the 1st step we obtain clear indication on range of the sought parameter (parameters) of the suppression circuit which have to be set in the simulation model, instead of selecting from the whole space, applying a trial and error method. The proposed design follows in the next two subsections.

3.2. ANALYSIS OF APPLICATION OF SUPPRESSION RESISTOR R_f

Assuming that the analysed CVT is equipped with a ferroresonance suppression resistance R_f (Fig. 4a) and neglecting the CVT load (thus more severe conditions for ferroresonance suppression are taken), the admittance $\underline{Y}_3$ defined in (9) equals:

$$\underline{Y}_3 = \frac{1}{R_f} + \frac{1}{R_e + j\frac{\omega L_e}{3} + \frac{3}{j\omega C_e}} \tag{23}$$

Substituting (23) into the condition (21) one obtains that to avoid stable subharmonic oscillations of the 3rd mode one has to apply:

$$R_f < 501.45 \text{ k}\Omega \tag{24}$$

This result clearly indicates that for the considered CVT construction (with parameters as specified in the subsection 3.1) the 3rd subharmonic oscillations are possible in case if it is not equipped with anti-ferroresonance suppression resistance, i.e.: $R_f = \infty$. This is confirmed in Example 1 at Fig. 6, where the selected recorded signals of the ATP-EMTP simulation are presented. Definitely, the transients of the 3rd subharmonic nature contained in the voltage and flux signals cause that the requirements of the standard are not satisfied. This calls for equipping the CVT with adequate anti-ferroresonance circuit.

The considered CVT construction is equipped with the anti-ferroresonance resistance of the value: $R_f = 367.5$ kΩ (which corresponds to 8.33 Ω resistor connected at the $100/\sqrt{3}$ side of the step-down transformer). The resistance of the damping resistor applied is of 73% of the border value obtained in the condition (24).

ATP-EMTP simulation-based analysis for this case is presented in Example 2 at Fig. 7. The initiated transients in the recorded secondary voltage are effectively damped in such a way that their influence on voltage magnitude is no greater than 10% after 175 ms since interrupting the short circuited secondary winding. The requirements imposed by the standard [9] are definitely satisfied.

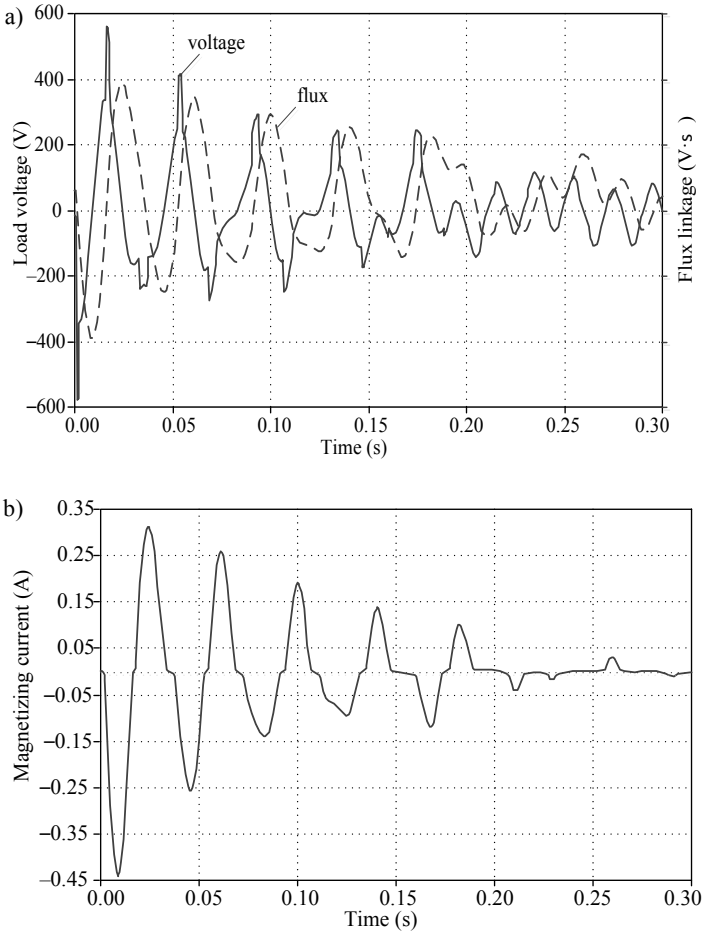

Fig. 6. Example 1 – The case of the ferroresonance test for the CVT construction with no anti-ferroresonance circuit: a) secondary voltage and flux linkage for the step-down transformer, b) its magnetizing current

The resistor R_f = 367.5 kΩ applied in the real considered CVT construction for suppressing subharmonic oscillations consumes 400 W power, which is quite big consumption in comparison to the nominal useful load (of protective and metering devices) which is designed to 150 VA. Moreover, such 400 kW permanent loading of the CVT by the anti-ferroresonance resistor is in all three phases. This is considered as a drawback of such way of damping nonlinear oscillations. From this reason it is considered further how to replace such damping resistor (Fig. 4a) with the circuit from Fig. 4b not consuming active power permanently, i.e. during steady state operation under fundamental frequency. The other option, which is not considered in this

paper, is based on applying a power electronic scheme which switches on the damping resistor only during transients, thus also not consuming active power during steady state operation under fundamental frequency.

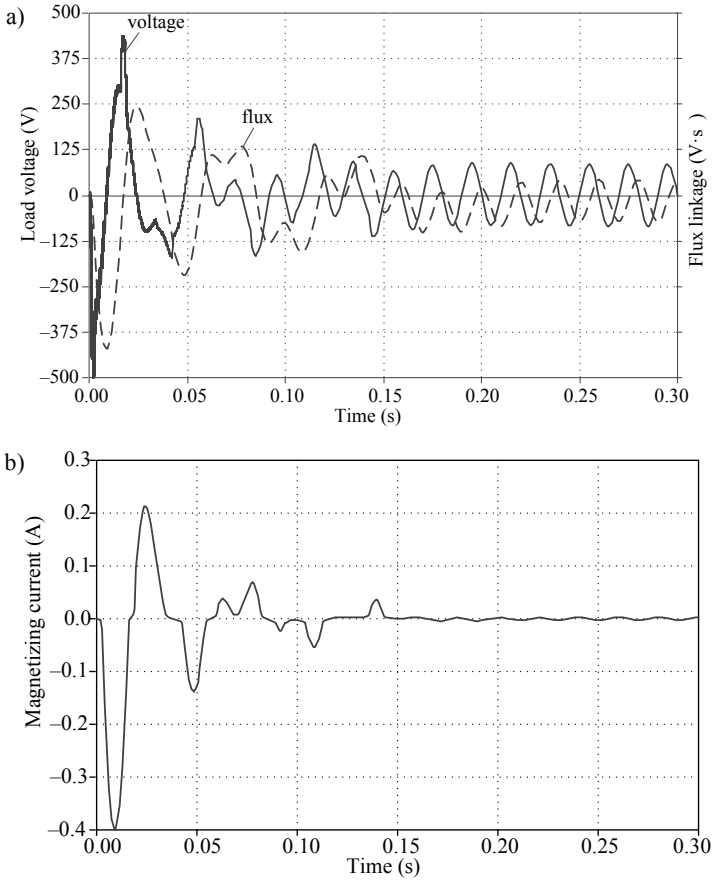

Fig. 7. Example 2 – The case of the ferroresonance test for the CVT construction with the suppression resistor $R_f = 367.5$ kΩ: a) secondary voltage and flux linkage for the step-down transformer, b) its magnetizing current

3.3. ANALYSIS OF APPLICATION OF SUPPRESSION CIRCUIT R_f L_f C_f

Assuming that the analysed CVT is equipped with a ferroresonance suppression circuit R_f L_f C_f (Fig. 4b) and neglecting the CVT load (thus more severe conditions for ferroresonance suppression are taken), the admittance $\underline{Y}_3$ defined in (9) equals:

$$\underline{Y}_3 = \frac{1}{R_\mathrm{f} - \mathrm{j}\frac{8}{3}\omega L_\mathrm{f}} + \frac{1}{R_\mathrm{e} + \mathrm{j}\frac{\omega L_\mathrm{e}}{3} + \frac{3}{\mathrm{j}\omega C_\mathrm{e}}} \tag{25}$$

When determining (25) it was taken into account that there is a tuning of L_f and C_f to the resonance at the fundamental frequency ($\omega^2 L_\mathrm{f} C_\mathrm{f} = 1$). For selecting the parameters of the considered suppression circuit it is assumed initially that the resistor R_f is not taking part in damping what imposes more severe conditions for the parallel connection of the elements L_f, C_f which are reactive elements and their influence is like 'increasing' the coefficient a_1 in the approximation (2), i.e. "making" the circuit more linear. Then, substituting (25) into the condition (21) one obtains that to avoid stable subharmonic oscillations of the 3rd mode the inductance L_f (recalculated for the voltage level of the primary side of the step-down transformer: $21000/\sqrt{3}$ V) has to satisfy:

$$L_\mathrm{f} < 1608.8\ \mathrm{H} \tag{26}$$

After few trials the value $L_\mathrm{f} = 1000$ H (around 60% of the border value from (26)) was taken for further analysis. Then, including the resistance R_f it has been found that there is optimal value of this resistance, i.e. the value for which the condition (21) is satisfied with the highest degree. By the term "highest degree" it is meant that the difference between the left and right sides of the inequality (21) is the highest. Thus, this feature has indicated that when carrying out the simulation based analysis for the assumed inductance ($L_\mathrm{f} = 1000$ H) one needs to search for the optimal value of R_f (Fig. 8: Example 3).

When searching for the optimal value of the resistance R_f of the circuit from Fig. 4b, the results as gathered in Table 1 have been obtained. They indicate that for the ratio $R_\mathrm{f}/(\omega L_\mathrm{f}) = 1$ the highest speed of damping is achieved. For the other values even no satisfying of the standard [9] is obtained, also including occurring stable 3rd subharmonic oscillations, what is marked by: $\propto$.

Table 1. Speed of Damping Nonlinear Oscillation Under the Ferroresonance Test of the CVT Equipped with the Suppression Circuit of Fig. 4b

L_f [H]	$\frac{R_\mathrm{f}}{\omega L_\mathrm{f}}$	Speed (ms)	Requirements satisfied?
1000	0.1	280	NO
	0.2	245	NO
	0.5	170	YES
	1.0	150	YES (optimal)
	2.0	375	NO
	5.0	$\propto$	NO
	10.0	$\propto$	NO

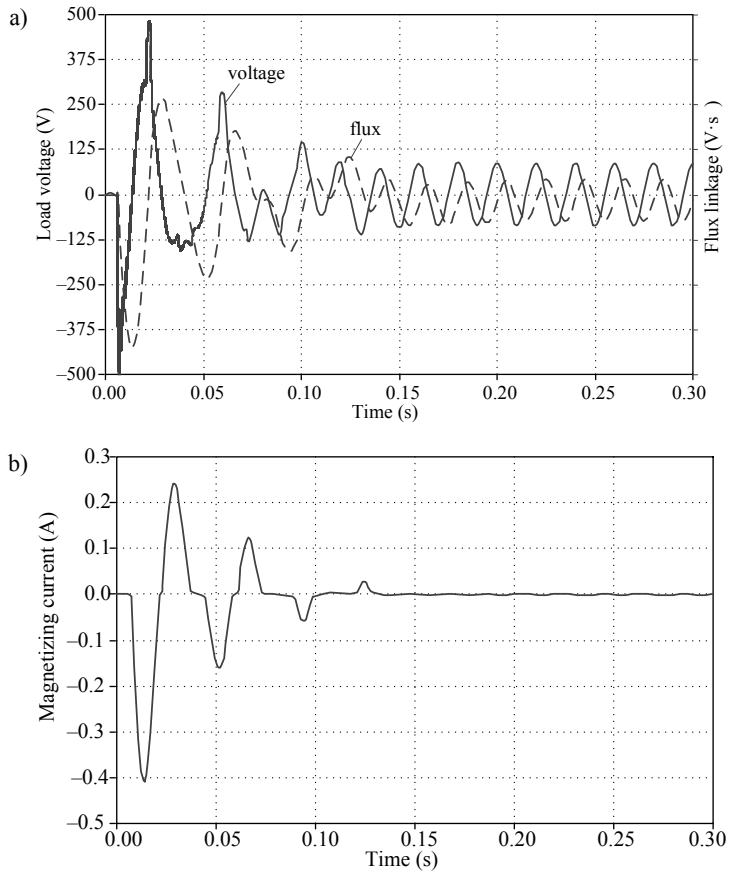

Fig. 8. Example 3 – The case of the ferroresonance test for the CVT construction with the selected suppression circuit $R_f L_f C_f$ (L_f = 1000 H, $R_f = \omega L_f$): a) secondary voltage and flux linkage for the step-down transformer, b) its magnetizing current

4. CHAOTIC OSCILLATIONS IN CVT

4.1. CLASSIFICATION OF FERRORESONANCE OSCILLATIONS

The foregoing analysis has shown that directly after the switching event in a CVT circuit, initial transient overvoltage will firstly occur and this is followed by the next phase of the transient where the process may come to at a more steady condition. Due to the non-linearity of the circuit, there can be several steady state ferroresonance responses. Depending on their spectral content, such oscillations are frequently classified as [16], [17]:

- Fundamental mode with periodic waveforms of the same period as the power system.
- Harmonic ferroresonance with periodic waveforms of a frequency multiple of the power system frequency.
- Sub-harmonic oscillations with periodic waveforms of a period sub-multiple of the power system period (with frequency of f_1/k, where: k – integer).
- Quasi-periodic ferroresonance: non-periodic waveforms with a discontinuous frequency spectrum (frequencies are defined as: $m_1 f_1 + m_2 f_2$, where m_1, m_2 – integers and f_1/f_2 is an irrational real number).
- Chaotic ferroresonance: non-periodic waveforms with a continuous frequency spectrum.

Different mathematical tools are employed to analyse the types of ferroresonance modes as: FFT or a Poincarè map [16]–[19]. The analysis given in the above sections is mainly related to sub-harmonic mode. The further part's scope is to investigate the chaotic oscillations and to identify a possible chaotic ferroresonance mode in CVT.

4.2. CHAOTIC OSCILLATIONS

Chaotic phenomenon in different physical systems is the subject of intensive study during the last several decades. Chaos (deterministic chaos) is a term used to designate the irregular behaviour of dynamical systems emerging from a strictly deterministic time evolution without any external source of fixed or probabilistic noise [20]–[22]. Such behaviour is typical for most non-linear systems. Aforementioned irregularity reveals itself in an extremely sensitive dependence on the parameters and initial conditions, which makes impossible any long-term projection of the dynamics. Mathematical tool for investigation of the chaotic phenomenon is the theory of dynamical system where an analysed system is represented by adequate set of differential equations [20].

To formulate such the equations for the CVT network let us consider the equivalent scheme as in Fig. 9, for which one can write:

$$\begin{aligned}
\frac{\mathrm{d}u_\mathrm{c}}{\mathrm{d}t} &= f_1 = \frac{1}{C} i_\mathrm{e} \\
\frac{\mathrm{d}i_\mathrm{e}}{\mathrm{d}t} &= f_2 = \frac{-1}{L_\mathrm{e}} \left(u_\mathrm{i} + u_\mathrm{c} + (R_\mathrm{e} + R_\mathrm{m}) i_\mathrm{e} + R_\mathrm{m} (i_\mathrm{b} / \vartheta + i_\mathrm{m}) \right) \\
\frac{\mathrm{d}i_\mathrm{b}}{\mathrm{d}t} &= f_3 = \frac{-1}{L_\mathrm{b}} \left((R_\mathrm{b} + R_\mathrm{m} / \vartheta^2) i_\mathrm{b} + R_\mathrm{m} (i_\mathrm{e} + i_\mathrm{m}) / \vartheta \right) \\
\frac{\mathrm{d}\psi_m}{\mathrm{d}t} &= f_4 = -R_\mathrm{m} (i_\mathrm{e} + i_\mathrm{b} / \vartheta + i_\mathrm{m})
\end{aligned} \tag{27}$$

where: $i_m = a_1\psi + a_{11}\psi^{11}$, a_1 = 4.28206e–5, a_{11} = 2.98252e–25; ϑ = 210 – transformation coefficient (the transformer is remained to compare results of calculations with simulations according to the model from Fig. 5). The switch *SW* initiates an initial condition – as in model of Fig. 5.

Equations (27) represent the non-autonomous continuous system of order $N = 4$ with external time dependent voltage source u_i. The system can be treated as autonomous one by adding explicit time dependent coordinate, obtaining $N + 1$ order system [23]. In this case the following equation was added: $\mathrm{d}\varphi/\mathrm{d}t = f_5 = \omega$, what leads to the voltage source of the form: $u_i = U\cos(\varphi(t))$ with: U = 18345.2 V, $\omega = 100\pi$ and $\varphi(0) = \pi/2$ (note that integration of this equation yields $\varphi(t) = \omega t + \pi/2$). The rest parameters of (27) are as in Subsections 3.1 and 3.2.

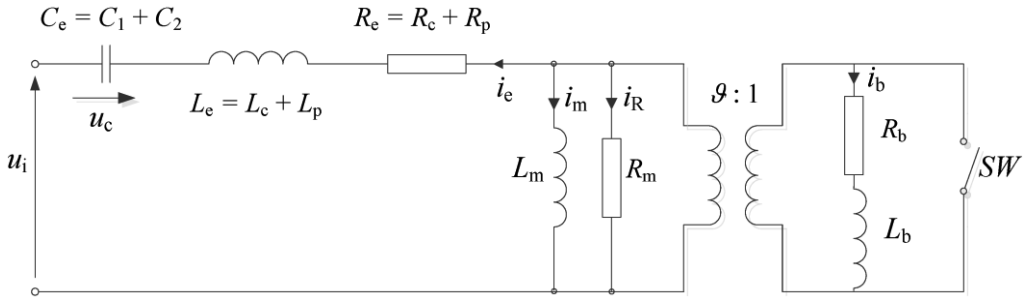

Fig. 9. Equivalent scheme of CVT

The system (27) was solved in MATLAB programme with application of the procedure `ode45` [24]. Fig. 10 gives a comparison between waveforms of the step-down flux linkage obtained from MATLAB calculation and ATP-EMTP simulation for the scheme without ferroresonance suppression circuit. One can see the significant differences in details of both the waveforms although their characters are very similar. The main source of these discrepancies is in a chaotic behaviour of the observed process. It is very sensitive to initial conditions, accuracy of a chosen integration method and other details e.g. a form of representation of the magnetizing characteristic which is different in the considered procedures: by the polynomial function $i_m = f(\psi)$ as in (27) – in the MATLAB programme, and by the piecewise-linear form – in the ATP-EMTP simulation [15].

4.3. DETECTION OF CHAOTIC PROCESS

A qualitative description of the behaviour of a non-linear circuit is usually demonstrated on phase plane. The observed trajectory gives an information on the system dynamics. This is characterised by the attraction areas to which the trajectory going

towards. It is known from the theory of dynamical systems that depending on the system features such areas can take forms of a single or various limit cycles (or even single point). Generally these cycles are called the attractors which are divided into the simple and the strange attractors [20]. Strange attractor is also called the chaotic attractor. Dynamics on the strange attractor is chaotic, and characterized by an extreme sensitivity to small changes in the initial conditions. For the computer simulated system it means that the calculation accuracy and the employed procedure also influences on the obtained waveforms.

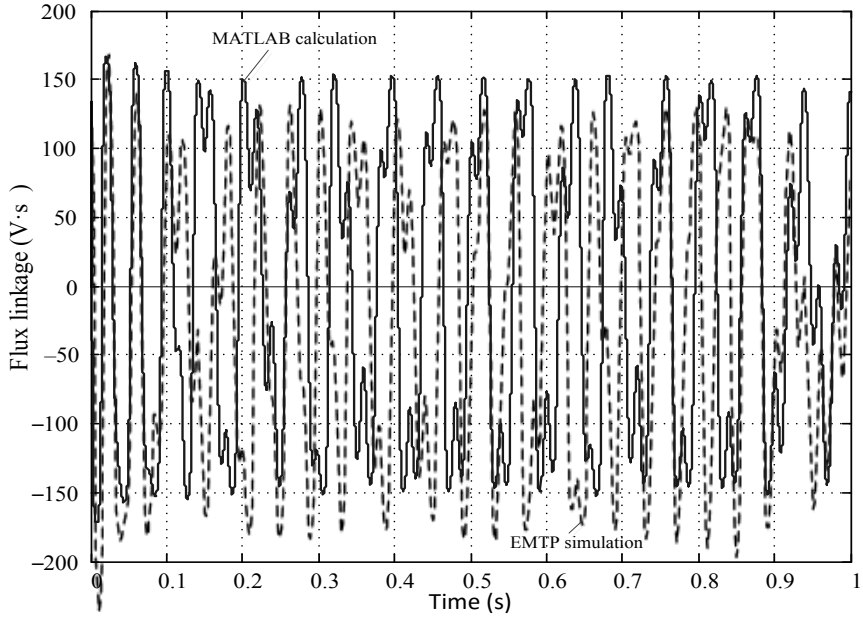

Fig. 10. Waveforms of flux linkage in step-down transformer (no suppression circuit)

As an example let us consider the phase plot in (u_c, i_e) plane for CVT scheme without the suppressing circuit (Fig. 11). After the initial transient period the trajectory evolves between two areas describing irregular cycles.

In the ferroresonant transients it is important to distinguish between the regular periodic fluctuations and the chaotic oscillations [19]. However it is easy to detect in this way a disappearance of the ferroresonance. The example is shown in Fig. 12. It is the similar phase plot as in Fig. 11 but for CVT circuit with the suppressing element in the form of resistance R_f as in Fig. 4a. One can see that after the initial transient period the trajectory describes the regular cycle for the steady state.

The chaotic evolution with a strange attractor is also characterized by so called self-similar properties, i.e., a form of a part of it is similar to the great-size (whole) set (as in fractal). Proper description of such features can be based on more general

analysis of the phase space of the system. The problem is solved by measuring the so called Lyapunov exponents or largest value from the spectrum of Lyapunov exponents [20]–[22].

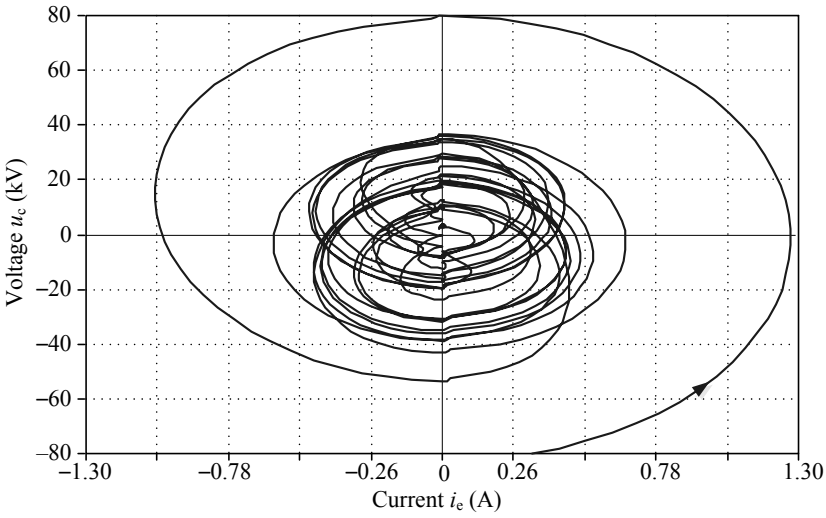

Fig. 11. Phase plot in (u_c, i_e) plane (CVT without suppressing circuit)

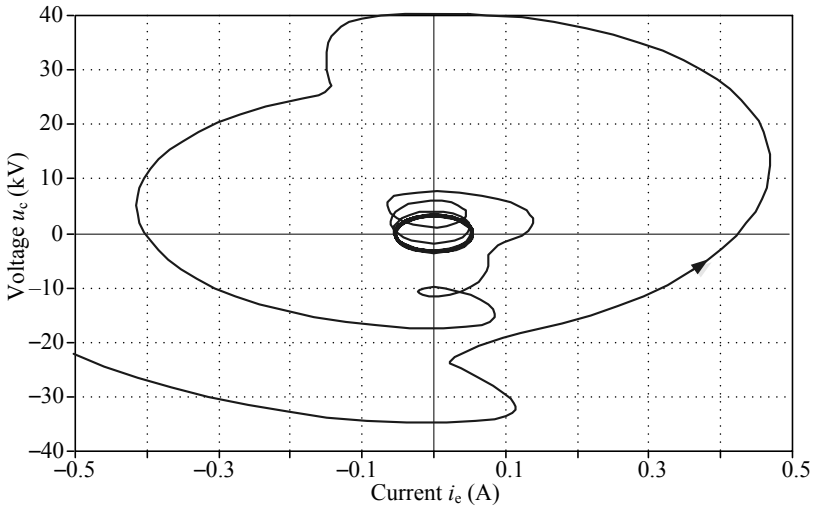

Fig. 12. Phase plot in (u_c, i_e) plane (CVT with suppressing circuit)

Lyapunov exponents quantify the exponential separation of initially close state-space trajectories and in that way characterize the amount of chaos in a system.

In a chaotic state the nearby trajectories (or initially close points) diverge exponentially, which can be quantitatively estimated by the Lyapunov exponent. The idea can be easily explained for one-dimensional discrete mapping at some interval [22]:

$$x_{n+1} = f(x_n) \tag{28}$$

Consider the evolution of (28) starting with slightly different initial conditions: x_0 and $x_0 + \Delta x_0$. The distance after n iterations can be defined as:

$$\Delta x_n = \left| f^n(x_0 + \Delta x_0) - f^n(x_0) \right| \tag{29}$$

For large n this can be estimated as [22]:

$$\Delta x_n \approx \Delta x_0 \mathrm{e}^{\lambda} \tag{30}$$

where λ is the Lyapunov exponent.

A positive Lyapunov exponent defines a chaotic trajectory. Normally, such a trajectory overlays a certain phase plane region and the Lyapunov exponent describes this region, regardless of the initial condition. Each coordinate in an N-order autonomous system described by a set of state equations can be characterized by separate Lyapunov exponent. Negative values of the Lyapunov exponent indicate stability, and positive values chaotic evolution, where λ measures the speed of exponential divergence of adjacent trajectories. The system is chaotic even if one Lyapunov exponent approaching positive value.

The methods for calculation of the Lyapunov exponents were the subject of the intensive research some years ago. Practical procedures can be found in the literature. They are adjusted to estimation of the Lyapunov exponent from the system equations [21], [22], [26] or from the recorded waveforms [21], [22], [25]. Employing the first mentioned procedure the user has to prepare a state model equations and adequate Jacobian of the transition matrix. Considering the CVT scheme with the equations (27) we can obtain:

$$\frac{\mathrm{d}}{\mathrm{d}t}\mathbf{x} = \mathbf{F}(\mathbf{x}), \qquad \mathbf{J}(\mathbf{F}) = \frac{\partial}{\partial \mathbf{x}}\mathbf{F} \tag{31}$$

where:

$$\mathbf{x} = \begin{bmatrix} u_c & i_e & i_b & \psi & \varphi \end{bmatrix}^T,$$

$$\mathbf{F}(\mathbf{x}) = \begin{bmatrix} f_1(\mathbf{x}) & f_2(\mathbf{x}) & f_3(\mathbf{x}) & f_4(\mathbf{x}) & f_5(\mathbf{x}) \end{bmatrix}^T,$$

$$\mathbf{J}(\mathbf{F}) = \begin{bmatrix} 0 & \frac{1}{C} & 0 & 0 & 0 \\ \frac{-1}{L_e} & \frac{-(R_e+R_m)}{L_e} & \frac{-R_m}{L_e\vartheta} & \frac{-R_m p_m}{L_e} & \frac{U\sin(\varphi)}{L_e} \\ 0 & \frac{-R_m}{L_b\vartheta} & \frac{-(R_b+R_m/\vartheta^2)}{L_b} & \frac{-R_m p_m}{L_b\vartheta} & 0 \\ 0 & -R_m & -R_m/\vartheta & -R_m p_m & 0 \\ 0 & 0 & 0 & 0 & 0 \end{bmatrix},$$

$$p_m = \frac{\mathrm{d}i_m}{\mathrm{d}\psi} = a_1 + 11a_{11}\psi^{10}.$$

All the network parameters are as in Subsections 3.1 and 3.2.

Details on the employed procedure in MATLAB can be found in [26]. The MATLAB programme adopted to the considered here CVT scheme is placed in [27].

Dynamics of the Lyapunov exponents for the CVT scheme without supressing circuit is presented in Fig. 13. After a short irregular transition the largest exponent λ_1 tends to value of 23.17 at the end of the showed section. The exponent λ_5 characterizes the regular component of angle φ and therefore is keeping of zero value. The exponent λ_4 takes a great negative value and is not presented in the figure.

Results of the Lyapunov exponents calculation for the same scheme but with the supressing circuit are presented in Fig. 14. This time, after a short transition the largest exponents λ_1 and λ_2 lead to some close negative values. This is typical for the stable network.

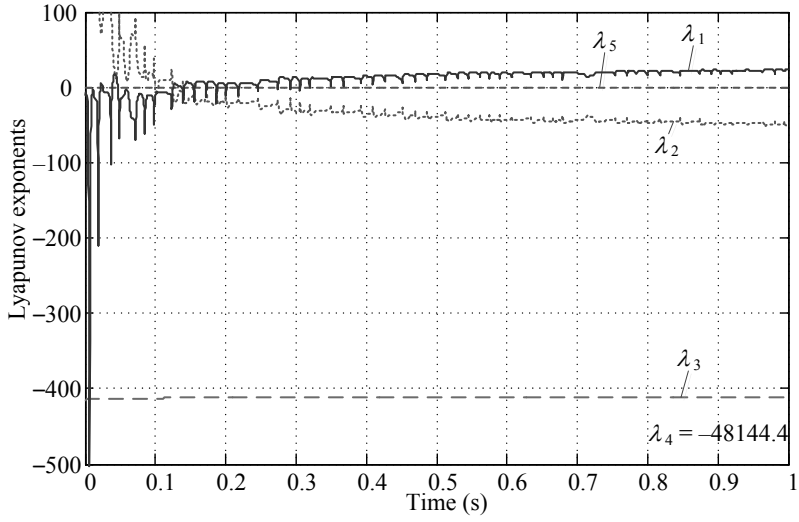

Fig. 13. Dynamics of Lyapunov exponents (CVT without suppressing circuit)

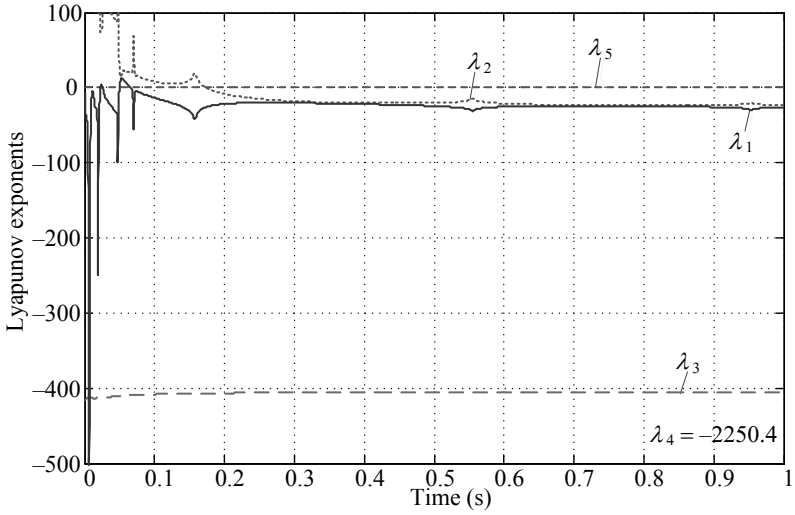

Fig. 14. Dynamics of Lyapunov exponents (CVT with suppressing circuit)

In the last calculation, the supressing circuit was included into the scheme in the form of the resistance R_f placed as parallel to the resistance R_m (Fig. 9). It is equivalent to simple reducing the value of R_m without any changing in the scheme and its set of equations.

5. CONCLUSIONS

Analysis of ferroresonance oscillations in CVT scheme has been presented. The main objective of the provided investigation was to formulate conditions for suppression of such oscillations. The 2-step procedure for designing the anti-ferroresonance suppression circuits for capacitive voltage transformers has been proposed.

The first step of the design is based on analytical approach to subharmonic ferroresonance of 3rd mode. The harmonic balance method and the 3rd order polynomial approximation of the nonlinear magnetizing characteristic have been applied. As a result, the condition stating when stable subharmonic oscillations of 3rd mode are not possible to occur has been derived.

The second step of the design is based on ATP-EMTP simulation of the ferroresonance test according to the national standard. Taking the condition derived in the first step, the final selection of the suppression circuit parameter (or parameters) is facilitated. Instead of selecting from the whole space for the parameters, the selection is to be carried out within the range where the parameters guarantee that stable subhar-

monic oscillations are not possible to occur. As a result of some limited trials the ferroresonance suppression circuit is designed to have desired speed of damping for nonlinear oscillations, i.e. as required by the standard.

Real, existing construction of CVTs has been taken for quantitative analysis. Two types of ferroresonance suppression circuits have been designed. It was shown that the presented analytical approach to subharmonic ferroresonance considerably facilitates the design of the ferroresonance suppression circuits.

Analysed ferroresonance oscillations can be divided into a few different modes depending on some specific time and spectral characteristics. It was shown that in the CVT scheme without supressing circuit one can also observe chaotic oscillations. Generally, chaotic ferroresonant behaviour depends on various parameters of the system: voltage source amplitude, capacitance and resistance, transformer core magnetic characteristic representation or initial conditions. Detection of chaotic phenomena can be provided by estimation of the Lyapunov exponents. It was shown that such oscillations can really exist in the CVT circuit.

ACKNOWLEDGMENTS

This paper was realized within NCBR project: ERA-NET, No. 1/SMARTGRIDS/2014, acronym SALVAGE, "Cyber-Physical Security for the Low-Voltage Grids".

REFERENCES

[1] ZADEH H.K., LI Z., *A compensation scheme for CVT transient effects using artificial neural network*, Electric Power Systems Research, 2008, 78, 30–38.

[2] SAHA M.M., IZYKOWSKI J., ROSOLOWSKI E., *Fault Location on Power Networks*, Springer, London 2010.

[3] ZANG W., SHU G., FENG Z., UNBEHAUEN R., *Digital simulation models of a capacitor voltage transformer*, Electrical Engineering, 2005, 87, 237–244.

[4] FERNANDES D. JR., NEVES W.L.A., VASCONCELOS J.C.A., *Coupling capacitor voltage transformer: A model for electromagnetic transient studies*, Electric Power Systems Research, 2007, 77, 125–134.

[5] BAKAR A.H.A., RAHIM N.A., ZAMBRI M.K.M., *Analysis of lightning-caused ferroresonance in Capacitor Voltage Transformer (CVT)*, Electrical Power and Energy Systems, 2011, 33, 1536–1541.

[6] MIGUEL A., OLGUÍN-BECERRIL, ANGELES-CAMACHO C., FUERTE-ESQUIVEL C.R., *Ferroresonance in subharmonic 3rd mode in an inductive voltage transformer, a real case analysis*, Electrical Power and Energy Systems, 2014, 61, 318–325.

[7] ABBASI A., SEIFI A., *Fast and perfect damping circuit for ferroresonance phenomena in coupling capacitor voltage transformers*, Elect. Power Compon. Syst., March 2009, Vol. 37, No. 4, pp. 393–402.

[8] CHAKRAPANIA V., SWARUP K.S., *Estimation of electronic suppression circuit resistance for protective relaying applications*, Electric Power Components and Systems, 43(3): 282–297, 2015.

[9] Polish Standard: PN-EN 61869-5:2011 – *Instrument transformers, Part 5: Detailed requirements for capacitor voltage transformers* (English version).

[10] IŻYKOWSKI J., WISZNIEWSKI A., *Damping of nonlinear oscillations in capacitive voltage transformers*, Przegląd Elektrotechniczny (Electrical Review), 1974, nr 1, pp. 20–23 (in Polish).
[11] IZYKOWSKI J., KASZTENNY B., ROSOLOWSKI E., SAHA M.M., HILLSTROM B., *Dynamic compensation of capacitive voltage transformers*, IEEE Trans. Power. Delivery, January 1998, Vol. 13, No. 1, pp. 116–122.
[12] KASZTENNY B., SHARPLES D., ASARO V., POZZUOLI M., *Distance relays and capacitive voltage transformers balancing speed and transient overreach*, Proceedings 53rd Annual Conference for Protective Relay Engineering, Ontario, Canada.
[13] COSTELLO D., ZIMMERMAN K., *CVT transients revisited distance, directional overcurrent and communications-assisted tripping concerns*, 65th Annual Conference for Protective Relay Engineers, College Station, TX, 2–5 April 2012, pp. 73–84.
[14] AJAEI F.B., SANAYE-PASAND M., DAVARPANAH M., REZAEI-ZARE A., IRAVANI R., *Mitigating the impacts of CCVT subsidence transients on the distance relay*, IEEE Trans. Power Del., April 2012, Vol. 27, No. 2, pp. 497–505.
[15] DOMMEL H., *ElectroMagnetic Transients Program*, BPA, Portland, Oregon, 1986.
[16] FERRACI P., *Ferroresonance*, Cahier technique no. 190, Groupe Schneider, March 1998.
[17] VAL ESCUDERO M., DUDURYCH I., REDFERN M.A., *Characterization of ferroresonant modes in HV substation with CB grounding capacitors*, Electric Power Systems Research, 2007, 77, 1506–1513.
[18] SOWA P., ŁUSZCZ K., *Chaotic behavior in a power system following ferroresonance*, Proceedings of the 14th International Scientific Conference Electric Power Engineering, 2013, pp. 79–82.
[19] FORDOEI H.R.A., GHOLAMI A., FATHI S.H., ABBASI A., *Chaotic oscillations control in the voltage transformer including nonlinear core loss model by a nonlinear robust adaptive controller*, Electrical Power and Energy Systems, 2013, 47, 280–294.
[20] SKIADAS C.H., SKIADAS C., *Chaotic Modelling and Simulation. Analysis of Chaotic Models, Attractors and Form*, CRC Press, Taylor & Francis Group, 2009.
[21] PARKER T.S., CHUA L.O., *Practical numerical algorithms for chaotic systems*, Springer-Verlag, 1989. Available in: http://link.springer.com/book/10.1007/978-1-4612-3486-9.
[22] KORSCH H.J., JODL H.-J., HARTMANN T., *Chaos. A Program Collection for the PC*, Springer-Verlag, Berlin, Heidelberg 2008.
[23] ALLIGOOD K.T., SAUER T.D., YORKE J.A., *Chaos – an introduction to dynamical systems*, Springer-Verlag, New York, Inc., 1996.
[24] *MATLAB user's guide*, The Math Works, Inc., 2000.
[25] ROSENSTEIN M.T., COLLINS J.J., DE LUCA C.J., *A practical method for calculating largest Lyapunov exponents from small data sets*, Physica D., 1993, 65, 117–134.
[26] KUZNETSOV N., MOKAEV T.N., VASILYEV P.A., *Numerical justification of Leonov conjecture on Lyapunov dimension of Rossler attractor*, Comm. in Nonl. Sci and Num. Simul., 2014, 19(4), pp. 1027–1034. The programme is also available in: http://www.math.spbu.ru/user/nk/PDF/Lyapunov-exponent-Sign-inversion-Perron-effects-Chaos.pdf
[27] *MATLAB programme for Lyapunov exponents calculation adopted to the CVT circuit*. Available in: http://zas.pwr.edu.pl/files